Initiating revolutions for optical manipulation: the origins and applications of rotational dynamics of trapped particles

Graham D. Bruce , Paloma Rodríguez-Sevilla & Kishan Dholakia

Published online: 23 Dec 2020.

Submit your article to this journal ↗

Article views: 255

View related articles ↗

View Crossmark data ↗

REVIEW   OPEN ACCESS   Check for updates

Initiating revolutions for optical manipulation: the origins and applications of rotational dynamics of trapped particles

Graham D. Bruce [ID][a]*, Paloma Rodríguez-Sevilla [ID][a]* and Kishan Dholakia [ID][a,b]

[a]SUPA School of Physics and Astronomy, University of St Andrews, St Andrews, UK; [b]Department of Physics, College of Science, Yonsei University, Seoul, South Korea

ABSTRACT

The fastest-spinning man-made object is a tiny dumbbell rotating at 5 GHz. The smallest wind-up motor is constructed from a DNA molecule. Picoliter volumes of fluids are remotely controlled and their viscosity precisely measured using microrheometers based on miniscule rotating particles. Theoretical predictions for extraordinarily weak forces related to the presence of dark matter, dark energy and vacuum-induced friction might be revealed, and the surprising properties of light have already been experimentally evidenced. All of these exciting landmarks have only been possible thanks to the torque exerted by light, which enables rotation of an optically trapped particle. Here, we review how light can impart torque on optically trapped particles, paying close attention to the design of the properties of both the particle and the light field. We detail how the maximum achievable rotation speed is limited by the environment, but can simultaneously be used to infer properties of the surrounding medium and of the light field itself. We also review the state-of-the-art applications of light-driven rotors, as well as proposals for the next generation of measurements, particularly at the classical-quantum interface, which can be performed using rotating optically trapped objects.

CONTACT Graham D. Bruce ✉ gdb2@st-andrews.ac.uk ✉ SUPA School of Physics and Astronomy, University of St Andrews, North Haugh KY16 9SS, UK; Kishan Dholakia ✉ kd1@st-andrews.ac.uk ✉ SUPA School of Physics and Astronomy, University of St Andrews, St Andrews, UK

*G. D. Bruce and P. Rodríguez-Sevilla contributed equally to this work.
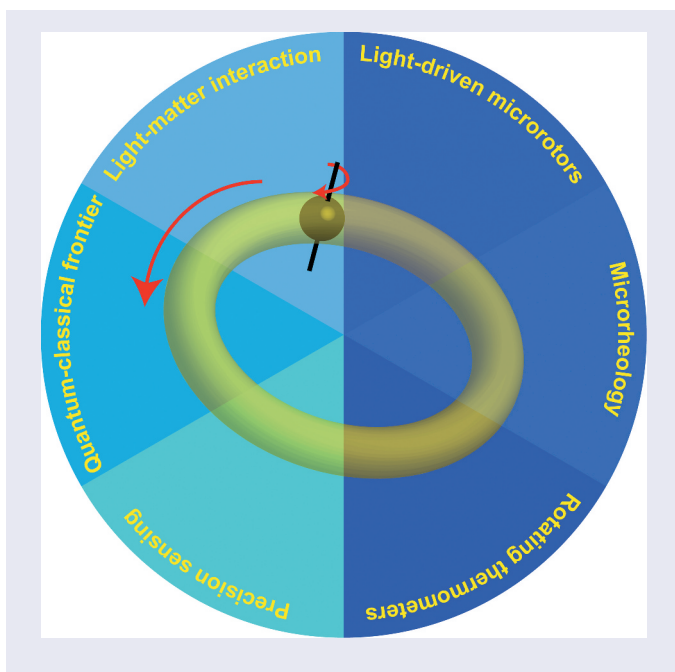
1. Introduction

One half of the Nobel Prize in Physics 2018 was awarded to Arthur Ashkin for his seminal development of optical tweezers. This technique uses focused beams of light to manipulate and confine mesoscopic objects using radiation pressure and gradient forces, which typically range from fN to pN [1]. While this is a small force, it is capable of stable trapping of dielectric and metallic particles ranging from tens of nanometers up to hundreds of micrometers. Such optical manipulation has found a diverse range of applications including studies in fundamental quantum physics and quantum computing with single atoms [2] to studying single-molecule biophysics [3], cells [4], and micro-organisms [5].

Optical trapping has been widely used for biological studies in liquid [6–9]. In a pioneering work, Ashkin *et al.* [4] proved that the judicious selection of the trapping wavelength and power enables the harmless optical manipulation of living cells, trapping yeast cells for several hours and observing their division and multiplication inside the optical trap. Thanks to the magnitude of the optical forces and the ability to perform precise displacement measurements below the nanometer level [7], optical trapping enables the study of subcellular entities such as DNA or molecular motors *in vitro*. For the latter case, the trap indirectly monitors the motion of the motor through the tethering of the molecule to a bead. A prime example is Kinesin, which is responsible for the

transport of vesicles through the volume of the cell. Optical trapping enabled the study of the motional dynamics of this molecular motor that 'walks' along intracellular filaments at a speed of ~ 0.5 µm/s [10], resolving its walking step of ~ 8 nm [11], and determining that it drags its cargo by exerting a force of ~ 1 pN [12]. Optical manipulation inside living cells [13] and even living animals [14,15] has been proven. Either endogenous or exogenous (whether inserted [16] or internalised [17,18]) material can be manipulated, which enables the *in situ* study of biological processes. Separately, optical tweezers in liquid environments has given major insights into several physical phenomena including thermodynamics. For example, adding thermal noise may show a Brownian nano-heat engine [19]. Two traps in close proximity create a double-well potential to explore the Kramers' transition rate [20]. Other exciting areas include optically induced organisation and particle dynamics in complex potential energy landscapes, which can mimic transport effects in atomic systems at the mesoscopic scale.

While there has been a large body of work over the last three decades trapping particles in liquid, optical manipulation of nano- and micro-particles in vacuum is increasingly providing exciting new directions for research. Optical trapping in low-pressure environments was first demonstrated by Ashkin in 1977 [21], but has been undergoing a rapid increase of interest in the last decade [22]. This has been primarily motivated by the fact that in a perfect vacuum, unlike in liquid environments, the levitated particle's motion is decoupled from the environment other than through its interaction with the laser. An early example of success in this area was the first explicit observation of ballistic Brownian motion [23], while a trapped particle can be used to detect forces on the zepto-Newton scale [24,25]. The isolation from the environment has opened the possibility to study quantum physics in new regimes of mass and size. This has stimulated many theoretical proposals for macroscopic quantum physics with optically levitated particles, e.g. [26–36]. This area of levitated optomechanics currently stands on an exciting threshold. After a decade of steady progress in methods to cool the centre-of-mass motion of levitated particles [37–43], the remarkable achievement of a levitated nanoparticle cooled to the ground state of its centre-of-mass motion [44] was reported earlier this year.

Much of the work in optical tweezers has initially concentrated on translational motion along the three Cartesian directions. However, an asymmetric feature of the particle or the use of structured light can also create *rotational* motion of the particle. This introduction of angular momentum has taken an increasingly prominent role in optical trapping. In this review, we will discuss the important questions around rotational motion in optical traps in both liquid and vacuum environments: how do we generate rotational motion, why do we generate rotational motion, and

what specifically in terms of new science can it engender? As we will see, rotation can have far-reaching consequences. For example, the development of miniaturised devices has benefited from light-activated rotors which can be harnessed as tiny pumps and actuators capable of controlling fluids [45] and triggering biological processes at the microscale [46]. In liquid media, rotating particles can be used for high precision measurement of intriguing physical properties of picolitre volumes of fluids [16] and the tiny torque exerted by small biological motors [47], and have given major insights into several physical phenomena including the angular momentum of light [48]. In high vacuum, nanoparticles have been shown to spin at rates up to 5 GHz [49]. At these rotation rates the forces on the particle are sufficiently high to test the material properties of the particle under extreme conditions [50]. Rotating asymmetric particles in vacuum may realise nanoscale torsion balances, which achieve unprecedented sensitivities to force and torque [49], offering an avenue to study open questions in fundamental physics such as whether the vacuum can exert friction on a moving body [51–53].

This review is structured as follows. We will first summarise the essential phenomena of translational motion in optical tweezers (Section 2), then provide an overview of the mechanisms by which trapped particles can be set into rotation (Section 3). We will discuss the key experimental questions of the fabrication of optimal particles for rotation, the maximum rotation speed that can be reached, and the detection of the rotational motion in Section 4. Finally, the new science and applications that emerge from exploiting this degree of freedom are discussed in Section 5.

2. Optical tweezers primer

Light exerts optical forces on matter which can typically be decomposed into two types: non-conservative scattering forces which depend on the intensity of light, and conservative gradient forces which depend on the gradient of the intensity. The scattering force results in radiation pressure along the direction of the light's wavevector k. For a transparent spherical particle with a higher refractive index than its surrounding medium, the gradient force attracts the particle to regions of highest intensity. In the ray optics regime, this may be considered as a result of the refraction of light within the sphere (see Figure 1).[1]

The most common configuration of stable, 3D optical trap is optical tweezers. This embodiment of optical forces uses a single Gaussian laser beam tightly focused by a high numerical aperture microscope objective (NA typically ≥ 1) to create an equilibrium point where the scattering and gradient forces balance in all three Cartesian directions.

A particle stably trapped in three dimensions will explore a region of the trap very close to this minimum energy position due to its Brownian motion. The force exerted on the particle may be approximated by considering
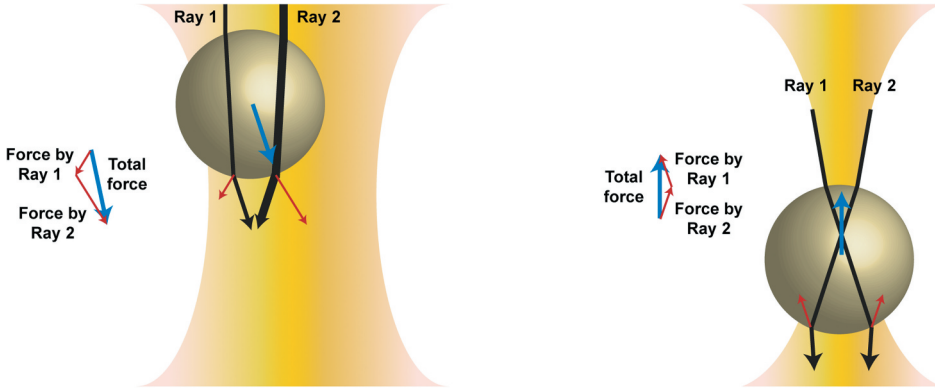
Figure 1. Origin of the optical force from a ray optics perspective. The refraction of the incident rays (black lines) produces a change in their linear momentum that in turn generates a reaction force (red arrows). Rays near the focus are more powerful, hence produce a strong reaction force. The net optical force (blue arrows) points towards the maximum intensity region in the beam's propagation direction. A weakly-focusing beam (left) exerts a transverse force much larger than the axial forces, while a tightly focused beam (right) is required for three-dimensional confinement.

separate linear restoring forces acting along each Cartesian direction: i.e. $F_q = -\kappa_q q$, where $q\epsilon\{x, y, z\}$ and κ_q is known as the trap stiffness. This is analogous to the spring constant of a Hookean simple harmonic oscillator, which optical tweezers mimics. In a linearly polarised trapping beam, the trap stiffness for each direction of translational motion is distinct. The trap stiffness is related to the natural oscillation frequency ω_q of the particle in the trap by $\omega_q = \sqrt{\kappa_q/M}$, where M is the mass of the particle.

Of course, the optical force is not the only force which acts upon the trapped particle. To incorporate a more complete picture of the motion, let us consider the equation of motion of the trapped particle (oscillator) along each Cartesian direction q. This is described by the Langevin equation

$$M\frac{\partial^2 q}{\partial t^2} + \gamma_q \frac{\partial q}{\partial t} + k_q q = F_{\text{fluct}}(t), \tag{1}$$

where the first term on the left-hand side is the inertial force on the particle, the second the velocity-dependent viscous damping force with γ_q the drag coefficient, and the third the optical force. The right-hand side is a stochastic force, F_{fluct}, due to Brownian motion arising from interactions with the environment, for which $\langle F_{\text{fluct}}(t) \rangle = 0$ and $\langle F_{\text{fluct}}(t_1)\, F_{\text{fluct}}(t_2) \rangle = 2k_B T_{\text{env}}\gamma_q \delta(t_1 - t_2)$. Here k_B is the Boltzmann constant and T_{env} the temperature of the environment. The trapped particle is a simple harmonic oscillator and, depending upon the environment, may be in the over-damped, underdamped or critical damping regime.

The magnitude of γ_q depends on the characteristics of the particle and, more importantly, on the properties of the environment. For a spherical particle trapped in a liquid medium of viscosity η, the drag coefficient is given by the Stokes law $\gamma_q = 6\pi a\eta$. In a gaseous environment, it is more common to consider $\Gamma_q = \gamma_q/M$, the pressure-dependent gas damping rate. For a sphere, this is [54]

$$\Gamma_q = \frac{6\pi a\eta}{M}\frac{0.619}{0.619 + \mathrm{Kn}}\left(1 + \frac{0.31\mathrm{Kn}}{0.785 + 1.152\mathrm{Kn} + \mathrm{Kn}^2}\right), \qquad (2)$$

where $\mathrm{Kn} = \hat{l}/a$ is the Knudsen number with $\hat{l} = (\eta/P_{\mathrm{gas}})\sqrt{\pi k_{\mathrm{B}}T_{\mathrm{env}}/2M_{\mathrm{gas}}}$ the mean free path of the gas molecules that have a mass M_{gas} and are at a pressure P_{gas}. As can be seen from Equation 2, Γ_q depends on the relative size of the particle compared to the mean free path of the gas molecules. This increases as the pressure decreases. At high pressure ($\mathrm{Kn} \ll 1$), the interaction between the particle and the gas molecules is so strong that the drag coefficient tends to the value given by the Stokes law. On the other hand, at low pressures when $\hat{l} \gg a$, the damping rate becomes linearly dependent on pressure

$$\Gamma_q^{\mathrm{Kn} \gg 1} \approx 3.714\frac{a^2}{M}\sqrt{\frac{2\pi M_{\mathrm{gas}}}{k_{\mathrm{B}}T_{\mathrm{env}}}}P_{\mathrm{gas}}. \qquad (3)$$

Due to this pressure-dependent damping, the behaviour of the particle is markedly different depending upon the medium in which it is suspended. When the particle is immersed in liquid, the viscous damping dominates over the inertial term and the particle undergoes overdamped oscillatory motion about its equilibrium point, subject to the effects of the Brownian motion. However, if the pressure is lowered, the inertial term becomes increasingly important and the motion of the particle becomes increasingly phase-coherent, parameterised by the quality factor $Q_q = \omega_q/\Gamma_q$. As the translational dynamics in both underdamped and overdamped regimes depend on Γ_q, this allows the particle to act as a sensitive probe of its environment, which can be used in areas including rheology, pressure sensing, and thermometry.

Equipped with these essential notions of translational motion in optical trapping, we now turn our attention to the *rotational* degrees of freedom.

3. Engineering rotational motion

Rotational motion of particles can be manifested in a variety of ways. The three main types of rotation are libration (also called torsion), spinning, and orbiting (Figure 2), which can be realised in any optical trapping system,[2]
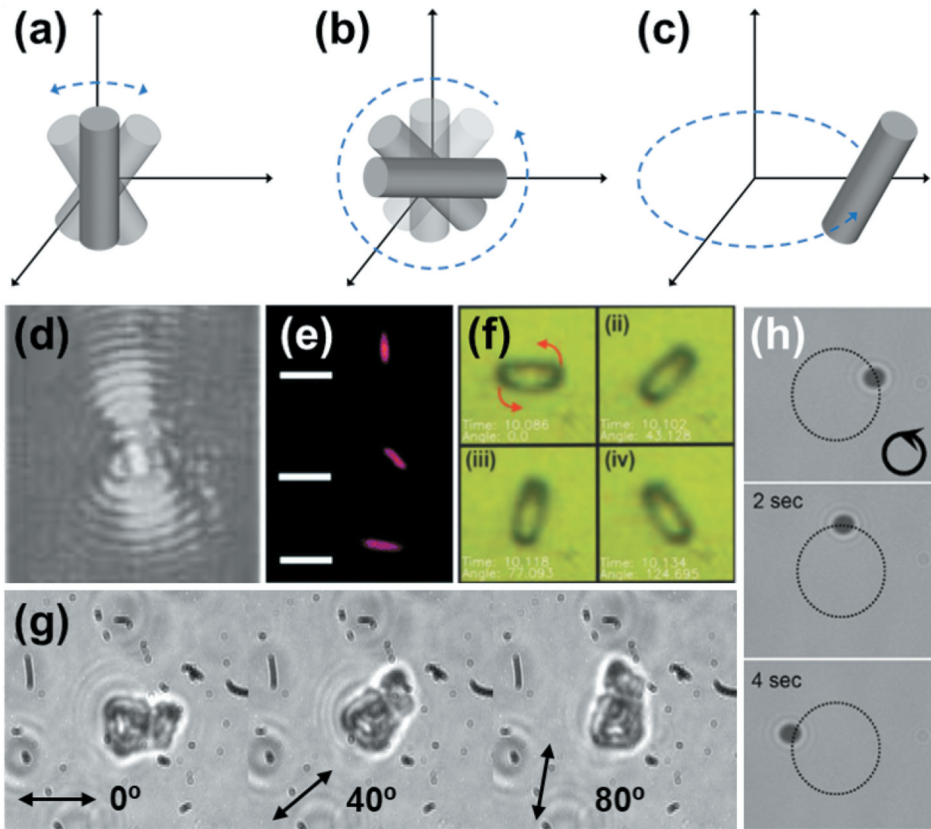
Figure 2. Types of rotation. Schematics of the three main types of rotational motion: (a) libration, (b) spinning, and (c) orbiting. (d) Librational motion and orientation of a disk can be detected from the scattered-light profile. Image adapted from [70]. Copyright (2002) by the American Physical Society. Asymmetric particles spinning (e) by the action of two independent traps that hold the particle from it ends (images adapted from [61] – Published by The Royal Society of Chemistry); (f) through transfer of spin angular momentum [151] (Copyright 2018 WILEY-VCH Verlag GmbH & Co. KGaA, Weinheim); and (g) by the action of the orientation torque when the linear polarisation is rotated (Adapted by permission from Springer Nature Customer Service Centre GmbH: Springer Nature, Nature [77],   1998). (h) A spherical particle undergoing orbital motion around the beam axis. Adapted with permission from [117]   The Optical Society.

such as free-space traps, cavities [55], near-field traps based on nanostructures [56], photonic crystal fibres [57] or evanescent fields created by fibres [58] or resonators [59]. In this section we will discuss how such rotational motion can be created.

Dynamic beam steering and shaping devices such as digital micromirror devices and spatial light modulators allow the creation of essentially any motion by dynamic manipulation of the position of optical traps. Apart from the trivial example of a particle trapped in a moving spot that describes a circular orbit [60], orientation and rotation of a particle can also be

achieved using multiple independent parallel beams. As an example, a cylindrical particle can be held from opposite ends and be rotated around its own axis by changing the relative location of the traps [61,62] (Figure 2 (e)). Similarly, customised rotors [45], constellations made of several entities [45], and living cells [63] have been spun using an array of optical traps that held the objects from specially designed or naturally occurring handles, allowing, for example, the precision control on the microscale of fluid flows generated by the optically driven rotors. Dynamic beam shaping devices can also be used to create more-complex rotating intensity distributions capable of trapping and moving particles. For example, rotating blade-shaped intensity distributions can be generated using the interference between Laguerre-Gaussian modes and plane waves [64] or modulated Moiré patterns [65], while optical Ferris wheels of rotating spots can be generated using interference of frequency-detuned Laguerre-Gaussian modes [66,67]. Similarly, the orientation of asymmetric particles can be controlled using spatial light modulators to generate so-called 'tug-of-war' optical tweezers where more than one high-intensity region pulls on the particle simultaneously [68].

Unstable trapping can also lead to rotation. A constant circulation motion of a silica microsphere can be produced by the interplay between conservative and non-conservative forces in a tightly-focused linearly polarised beam [69]. For asymmetric particles such as disks [70,71] and ellipsoids [72], a *tumbling* motion can be generated by unstable trapping. For example, when the particle is trapped in close proximity to an extended surface, the particle tilts from a stable position due to increased asymmetric drag near the wall [73] and undergoes a periodic pendular motion perpendicularly to the laser polarisation.

While optical trapping relies on the transfer of linear momentum from light to the particle, rotation may also be engineered by transferring angular momentum from light to the particle. This can be either spin angular momentum (associated with the light's circular polarisation) or orbital angular momentum (associated with inclined wavefronts of the light).[3] Non-spherical particles experience a torque due to scattering or absorption. However, the dynamics can be complex, and knowledge of the relevant drag torque is limited to special cases such as rods, ellipsoids and dumbbells [74,75]. In order to perform quantitative analysis of the rotation to perform some measurement of the environment (in analogy to measurements performed with translation), it is often preferable to impart angular momentum onto a symmetric body. If the trapped object is birefringent, this alternative form of anisotropy can be used to place a spherical object into rotation via transfer of spin angular momentum from circularly polarised trapping light. Even non-birefringent spherical objects can be put into rotation by transfer of orbital angular momentum from structured light to the particle, mediated

by scattering or absorption. In general, the total optical torque exerted on a particle will have contributions due to more than one property of the particle (i.e. it may be birefringent, partially absorbing and non-spherical), while the light may also contain both spin and orbital angular momentum. In all cases, the maximum rotation rate that can be realised will depend on the properties of the environment, as the particle will reach a terminal angular velocity due to the balance between the applied optical torque and the friction torque produced by the surrounding medium.

In the remainder of this section, we will investigate the instigation of rotation in detail. We begin with a discussion of how each of the three main forms of rotation can be realised in a single light beam carrying angular momentum. Libration and spinning are mostly related to the interaction of anisotropic (Section 3.1) or absorbing (Section 3.2) particles with the polarisation of the light, while orbiting (Section 3.3) is usually generated by scattering of structured light beams that carry orbital angular momentum. In many experimental configurations the fundamental torques that arise from the transfer of angular momentum in a free-space trap are insufficient to describe the motion of the particle when, for example, there is an interplay between the angular momentum components (Section 3.4). Many alternative geometries of optical traps exist beyond single-beam, free-space optical tweezers. These may offer advantages for particular applications, and we will briefly show how rotational motion can be realised in some of these other trapping geometries in Section 3.5. Finally, intriguing phenomena such as optical binding can arise when multiple particles are held in a single optical trap, and we will discuss the implications for the rotational motion in Section 3.6.

3.1. Anisotropy-induced torque

For a non-absorbing particle whose size is of the order or smaller than the trapping wavelength, the optical torque $\tau_{\mathbf{opt}}$ is mainly governed by the interaction of the electric field $\mathbf{E}$ of the light with the susceptibility χ of the particle. Specifically, $\tau_{\mathbf{opt}} = \langle \mathbf{P} \times \mathbf{E}^* \rangle$, where $\mathbf{P} = \chi \mathbf{E}$ is the induced polarisation [76]. If the particle is not isotropic, e.g. it has an internal birefringence or presents a non-spherical shape, its susceptibility is a tensor and one can define three principal axes ($\hat{x}$, $\hat{y}$, $\hat{z}$) so that $\mathbf{P} = \chi_x E_x \hat{x} + \chi_y E_y \hat{y} + \chi_z E_z \hat{z}$. For a birefringent particle, χ_x, χ_y, and χ_z will be the susceptibilities along the axes of the crystal, that will be reduced to only two (the ordinary χ_o and extraordinary χ_e axes) in a uniaxial crystal such as vaterite or quartz (see Section 4.1.1). When polarised light passes through such a particle, the ordinary and extraordinary component of the light undergo different orientation-dependent phase shifts. This results in

a change of the spin angular momentum of the light that produces a reaction torque [77,78]

$$
\begin{aligned}
\tau_{\text{opt}} = & -\frac{\epsilon}{2\omega_{\text{laser}}} E_0^2 \sin(kd(n_{\text{o}} - n_{\text{e}}))\cos2\phi\sin2\theta \\
& + \frac{\epsilon}{2\omega_{\text{laser}}} E_0^2 (1 - \cos(kd(n_{\text{o}} - n_{\text{e}})))\sin2\phi,
\end{aligned}
\tag{4}
$$

where E_0 is the amplitude of the electric field, ϵ is the permittivity of the particle, d its thickness, n_{o} and n_{e} the refractive indices experienced by the ordinary and extraordinary light, respectively, k the free space wavenumber, ω_{laser} the frequency of the light, and ϕ its degree of polarisation ellipticity ($\phi = 0, \pi/2$ represents linearly polarised light and $\phi = \pi/4$ circularly polarised light).

The magnitude of the optical torque depends on the change produced by the particle on the polarisation state of the light (i.e. retardation), which is proportional to the birefringence of the particle $\Delta n = n_{\text{o}} - n_{\text{e}}$ and the ratio of the trapping wavelength λ_{laser} to the particle's thickness, i.e. $kd = 2\pi d/\lambda_{\text{laser}}$. Therefore, for a specific trapping wavelength, the properties of the particle can be tailored to maximise the applied optical torque. We will discuss these experimental considerations in more detail with specific examples in Section 4.1.

For a non-spherical particle with two main polarisable axes, e.g. a cylindrical particle, a *shape-induced* birefringence can be similarly defined along the major and minor axes (see Section 4.1.3). In this case, the torque arises due to asymmetric scattering forces when the principal axis of the particle is not parallel to the light's electric field. Calculating the forces on a non-spherical particle is, in general, challenging and often performed numerically [79]. However, in the limit where at least one dimension of the particle is significantly smaller than the wavelength of the light (the Rayleigh-Gans limit), analytical solutions can be found [74,75].

The optical torque in Equation 4 can be responsible for distinct dynamics of the particle. For the case of pure linear polarisation, the second term vanishes and the particle undergoes librational or torsional oscillations around an equilibrium orientation (see Section 3.1.1). On the other hand, for the case of pure circular polarisation, the first term is zero and the particle undergoes continuous rotation around its own axis (see Section 3.1.2).

3.1.1. Libration

For an anisotropic, non-absorbing particle with two main polarisable axes trapped in *linearly* polarised light ($\phi = 0, \pi/2$), only the first term of Equation 4 survives, therefore the optical torque acting on the particle is

$$\tau_{\mathrm{opt}} = -\frac{\epsilon}{2\omega_{\mathrm{laser}}}E_0^2\sin(kd(n_{\mathrm{o}} - n_{\mathrm{e}}))\sin 2\theta.\qquad(5)$$

This is called the *orientation* torque, and it vanishes when the main axis of the particle and the polarisation are aligned ($\theta = 0$). Therefore, in a linearly polarised optical trap, an anisotropic particle aligns to the polarisation vector of the light, experiencing a restoring torque $\tau_{\mathrm{opt}} = \kappa_\theta\theta$ which is linear in the orientation angle θ to first order. The particle undergoes libration, which is a harmonic motion about the polarisation axis with a spring constant κ_θ which linearly increases with the trapping power. Alignment and librational motion have been demonstrated in over- and under-damped conditions for a wide range of particles such as fluorinated polyimide microparticles [80], wax microdisks [70] (Figure 2(d)), nanodumbbells [81], anisotropic diamond crystals [75], nanofabricated silicon cylinders [82], YLF crystals [83], and non-spherical birefringent $NaYF_4$ particles [18].

As another example of a harmonic oscillator, the librational modes of oscillation share many features with the translational modes. When the particle is trapped in liquid media, this harmonic oscillation is 'hidden' due to the thermal-induced Brownian motion, the same way as in the translational motion. This thermal noise imposes a minimum to the optical torque that can be exerted and detected. The limit reduces in the under-damped regime, as the gas pressure is reduced, and becomes negligible in high vacuum conditions where the minimum torque is then limited by the shot noise of the laser beam [81] (see Section 5.5). In optical levitation experiments, the librational modes of oscillation exist at higher frequencies than the translational modes, because while $\omega_{\mathrm{q}} = \sqrt{\kappa_{\mathrm{q}}/M}$ for vibration, for librational motion the oscillation frequencies are $\omega_\theta = \sqrt{\kappa_\theta/I}$, i.e. they depend on the moment of inertia I, which is proportional to the fifth power of the particle's radius a^5 for a sphere (as opposed to mass M which is proportional to a^3). Hoang *et al.* [75] measured a librational frequency of non-spherical nanodiamonds ($\omega_\theta = 1$ MHz) that was almost one order or magnitude larger than the frequency of the translational modes for the same trapping power. These librational frequencies often lie where the noise floor of the particle's position spectrum is lower, which enables lower detection limits. Moreover, the higher frequency of the libration means the quantum ground-state energy of the librational mode will be higher than for translational modes for the same optical power, which may be advantageous for cooling particle motion to quantum states [84] (see Section 5.6).

The control over the alignment of the particle can be used to enhance the light–particle interaction, e.g. to increase the percentage of laser power absorbed by the particle [83] (Section 5.4), while the librational motion can be used to study properties of the environment such as

viscosity [18] (Section 5.3) and the temperature of the particle itself [83] (Section 5.4).

3.1.2. Spinning

In the previous section we have seen that anisotropic particles align to the polarisation axis in a linearly polarised optical trap. If the polarisation angle rotates, the particle is forced to follow its motion due to the orientation torque (Equation 5) and it rotates around its own axis [76,77,85,86] (Figure 2(g)). For clarity and consistency, in this review we call this motion *spinning*. Rotating the polarisation is a simple way to produce spinning, however the achievable rotation speeds are limited by the rate at which the linear polarisation of the light can be rotated and the ability of the particle to follow the polarisation. For example, Bonin *et al.* [85] observed continuous rotation of 2–5 μm-long borosilicate glass fibres in liquid medium when the rotation rate of the linear polarisation was below 1 Hz. Above that threshold, the microfibers underwent *rocking* motion, i.e. rotated back and forth over a finite angular range. In both situations, the rotation rate of the particle matched the one of the polarisation, however, for much higher polarisation rotation rates, the particles locked at an angle, unable to follow the polarisation of the light.

If, instead of linearly polarised light, the anisotropic non-absorbing particle with two main polarisable axes is trapped by circularly polarised light ($\phi = \pi/4$), the first term in Equation 4 vanishes, and the particle experiences a torque which is independent of the orientation angle:

$$\tau_{\text{opt}} = \frac{\epsilon}{2\omega_{\text{laser}}} E_0^2 (1 - \cos(kd(n_{\text{o}} - n_{\text{e}}))). \tag{6}$$

The alignment-independence means that this torque is non-conservative, and the particle is therefore subjected to constant rotational driving and undergoes a spinning motion at a rate determined by the balance between optical torque and drag torque (see Section 4.2).

It is important to notice that, when the light is elliptically polarised (as is usually the case in experiments), both terms of Equation 4 play a role. A particle will only undergo continuous spinning when the circular portion of the polarisation is larger than the linear portion [87], i.e. the rotation torque (Equation 6) is larger than the orientation torque (Equation 5). Thus, there is a minimum ellipticity value that will produce rotation. Again, the particle may not spin due to the environmental conditions, as outlined above for the case of spinning in linearly polarised light and discussed in Section 4.2.

The transfer of spin angular momentum from light to a mechanical object was first demonstrated by Beth [88] in 1936. In this seminal work, he measured a 0.1 fN m torque produced by the change in the angular momentum of

polarised light passing through a one-inch diameter birefringent plate made of quartz, and confirmed that his results agreed with the predictions made by both the electromagnetic and quantum theories of light. Even replacing Beth's tungsten lamp with a few milliwatts of laser power would only produce a torque sufficient to make an one-inch diameter, 1 g waveplate undergo one full rotation every 8 months! These numbers might make one think that Beth's result may have just been a curiosity, but decades later, it was demonstrated that the phenomenon proved by Beth can be used to induce a substantial torque on optically trapped microscopic particles. Illuminating 12 μm-diameter calcite particles dispersed in distilled water with 50 mW of laser light, Friese *et al.* demonstrated rotation rates of over 350 Hz [77].

3.2. Absorption-induced spinning

Now imagine a perfectly spherical non-birefringent particle trapped in a circularly polarised beam. In this situation, spin angular momentum can only be transferred to the particle through *absorption* [89,90]. Marston *et al.* [91] calculated the time-averaged torque caused by a circularly polarised plane wave on a homogeneous isotropic sphere to be

$$\tau_{\text{opt}} = \frac{I_{\text{laser}}\sigma_{\text{abs}}}{\omega_{\text{laser}}}\sigma_{\text{z}}, \tag{7}$$

where I_{laser} is the laser irradiance and $\sigma_{\text{abs}} = \pi a^2 Q_{\text{abs}}$ the absorption cross-section of the particle, with Q_{abs} the absorption efficiency. We have introduced the dependence on the polarisation state σ_{z} of the light ($\sigma_{\text{z}} = \pm 1, 0$ for circularly and linearly polarised light, respectively) to stress that the torque is proportional to the spin angular momentum $\sigma_{\text{z}}\hbar$ carried by the photons, and highlight that there is no contribution from this torque when the light is linearly polarised. This is in contrast to the case of the torque due to the anisotropy of the particle (Section 3.1), in which the linear and circular portions of an elliptically polarised beam affect the rotation of the particle.

For an absorbing particle trapped in circularly polarised light, the magnitude of the optical torque only depends on the capacity of the particle to absorb the incident light. For a highly-absorbing particle much larger than the trapping wavelength, $Q_{\text{abs}} \simeq 1$ is theoretically expected [91]. That was the favourable situation that allowed the first observation of absorption-induced rotation for microscopic CuO particles [89]. For smaller particles the absorption cross-section is reduced, decreasing the amount of laser power absorbed by the particle. However, sub-wavelength metallic particles can support surface plasmon resonances that increase Q_{abs} at particular wavelengths determined by their dimensions and the dielectric properties of the environment. Thus, metallic nanoparticles spin at a rotation rate strongly dependent on the surrounding medium, which makes them ideal

candidates for sensing applications, e.g. the detection of the attachment of molecules to the particle surface, which modifies both the local viscosity and plasmonic response of the particle [92].

Absorption of light is frequently linked to heating, which usually needs to be avoided due to the structural changes that the temperature increase can produce to the environment or the spinning particle itself. This limits the power range that can be used, hence placing a ceiling to the rotation rates that could be achieved. This drawback is particularly relevant when the particle is levitated in gaseous environments and the heat dissipation mechanism are highly inefficient [93]. Nevertheless, this temperature increment enables the study of non-equilibrium hydrodynamics (see Section 5.4), and can be harnessed to create faster rotations (see Section 5.2) as the viscosity of the environment reduces (see Section 4.2).

3.3. Orbital motion

An object can undergo a curved trajectory around a point outside its own volume if the acceleration (net applied force) is not parallel to its velocity. In a light field with inclined phase fronts, the wavevector k is no longer parallel to the propagation axis of the beam (see Figure 3(a,b)). This leads to a scattering force which creates transverse momentum of the particle, and can be harnessed to produce orbital motion of a trapped particle around a closed circuit.
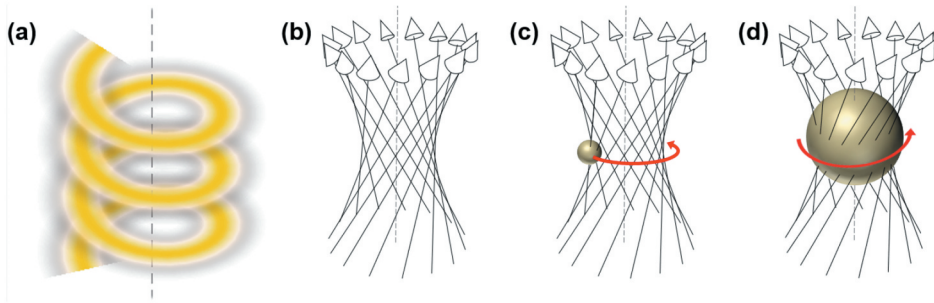

Figure 3. Rotational motion induced by orbital angular momentum. (a) Schematic showing the 'twisted' isophase of a Laguerre–Gaussian beam, where the colormap shows the beam intensity at each position. (b) The wavevector of a Laguerre–Gaussian mode is not parallel to the propagation direction of the beam, but can be visualised by considering a skew ray picture (figure modified from [94], Copyright (2000), with permission from Elsevier). The arrows show the direction in which the scattering force acts, while the gradient force pulls the particle to the location of maximum intensity. (c) When the particle is smaller than the spatial extent of the beam, it is trapped in the ring of maximum intensity and orbits around the beam propagation direction. (d) However, if the particle is larger than the spatial extent of the beam it is trapped on the central beam-axis and spins.

The most common method to create a closed trajectory is to illuminate the particle with a Laguerre–Gaussian beam. In contrast to zero-order Gaussian beams, Laguerre–Gaussian modes may have azimuthally inclined phase fronts. From a ray-optics perspective, these wave fronts can be seen as skew rays that point perpendicularly to the phase front [94] (Figure 3(b)). As k now has a component in the azimuthal direction around the beam's optical axis [95], scattering or absorption causes a particle trapped in such a beam to undergo a circular motion around the beam axis.

These tilted phase fronts are associated with the orbital component of the angular momentum of the light. Allen *et al.* [96] mathematically demonstrated that a Laguerre–Gaussian laser mode has a well-defined orbital angular momentum $\ell\hbar$ per photon encoded in the transverse profile of the beam, through a phase component of the form $\exp(i\ell\phi)$. Here ℓ is known as the azimuthal mode index or topological charge, which takes positive or negative integer values and is the number of 2π phase windings the electric field undergoes over a single wavelength. (In general, any beam with tilted phase fronts carries orbital angular momentum about the beam axis [97].) A Laguerre-Gaussian beam has zero intensity in the centre due to the presence of this optical vortex, and therefore the intensity forms a ring-profile. The radius r_ℓ of the ring increases with the topological charge (i.e. $r_\ell = \sqrt{z_\ell \ell/k}$, with z_ℓ the Rayleigh range of the beam), and can therefore be tuned in an experiment.

A particle can be trapped by the gradient force at the radius of maximum intensity.[4] Orbital rotation around a circular path following the beam profile is induced if the particle is trapped off-axis (Figures 3(c and 2(h)), i.e. in a beam with a spatial profile much bigger that the particle size [95,97–101]. On the other hand, particles larger than or comparable to the spatial extent of the beam profile can be trapped on the beam axis and spin [102,103] (Figure 3(d)). This phenomenon led He *et al.* [102] to observe for the first time the transfer of orbital angular momentum to particles made of super-conductive ceramic and cupric oxide trapped in a linearly polarised $\ell = 3$ Laguerre-Gaussian beam. This is interesting as it offers an avenue to realise spinning motion for low-absorption, perfectly spherical, non-birefringent particles, to which spin angular momentum of light cannot be transferred efficiently (see Sections 3.1 and 3.2).

The optical torque produced by orbital angular momentum transfer is analogous to that exerted on an absorptive particle by spin angular momentum transfer (see Equation 7), but proportional to the orbital angular momentum of the beam [89,95]

$$\tau_{\text{opt}} = \frac{I_{\text{laser}}(\sigma_{\text{abs}} + \sigma_{\text{scat}})}{\omega_{\text{laser}}}\ell, \tag{8}$$

with σ_{scat} the scattering cross-section, which usually dominates over σ_{abs} [100,104]. In contrast to the transfer of spin angular momentum, a larger torque can be applied per photon due to the fact that ℓ can take values much greater than one.

The application of torque due to the orbital angular momentum of light places no particular demands on the characteristics of the particle itself, i.e. it can be applied to particles without the requirement of high absorption, non-sphericity or intrinsic birefringence. Instead, what is required to generate the torque is control over the phase and amplitude of the light.[5] The generation of such structured light is exceptionally well-reviewed, see e.g. [48,105–110], due to applications across disparate fields of optics (see [111,112] for roadmaps of this area).

3.4. Interplay between spin and orbital angular momentum

The properties of the light and the way it illuminates the particle, together with the characteristics of the latter, will determine whether both, just one or none of the angular momentum components are transferred to the particle and hence influence its motion [101,103,113]. Thus, the main mechanism which transfers angular momentum from radiation to matter strongly determines the behaviour of the particle. For example, scattering and absorption of the light play a role in the transfer of orbital angular momentum (see Equation 8), while spin angular momentum can only be transferred to a spherical, non-birefringent particle through absorption (see Section 3.2). This is relevant when the beam carries both components but has zero total angular momentum (i.e. the spin and orbital angular momentum have equal magnitude but opposite sign). For example, a Laguerre-Gaussian beam with a spin angular momentum of -1 and a topological charge of 1 can still induce the rotation of a spherical, non-birefringent, and non-absorbing particle [98], because the polarisation state has no influence on the scattering force responsible for the transfer of orbital angular momentum. Thus, the dynamics of the particle can be used to determine the nature of the interaction between the particle and the light, and as a probe of the light field (see Section 5.1).

For a highly absorbing particle (i.e. $\sigma_{\text{scat}} \ll \sigma_{\text{abs}}$), spin and orbital angular momenta are transferred with the same efficiency (i.e. the optical torque equals the sum of Equations 7 and 8) so that the applied torque is proportional to the transfer of total angular momentum $(\sigma_z + \ell)\hbar$ [97]. Thus, for such a particle in a circularly polarised Laguerre-Gaussian beam, the optical torque and hence the rotation frequency increases (decreases) when the spin and orbital angular momentum of the light have the same (opposite) sign [89,103].

This may make one think that an absorbing particle in a circularly polarised Laguerre-Gaussian beam with zero total angular momentum would not rotate. However, this is not the case since the two components of the angular momentum are decoupled only in the paraxial approximation ($kz_\ell \gg 1$). When the beam is focused, as is common in optical trapping, a non-paraxial theory is necessary to describe the system which leads the appearance of a mixing term in the optical torque [89]

$$\tau_{\text{opt}} = \frac{I_{\text{laser}} \sigma_{\text{abs}}}{\omega_{\text{laser}}} \left[(\sigma_z + \ell) + \sigma_z \left(\frac{2kz_\ell}{2p + \ell + 1} + 1 \right)^{-1} \right], \qquad (9)$$

where $(p + 1)$ is the number of radial nodes of the Laguerre-Gaussian mode.

The interplay of the two components of the angular momentum can be advantageous. For example, the polarisation can be used to stabilise a particle orbiting along the high-intensity ring of a Laguerre-Gaussian beam in liquid media. If circularly polarised light is used, the gradient forces generated by the Laguerre-Gaussian beam exhibit circular symmetry in the radial direction around the optical axis, which favours a better confinement of the particle along the whole trajectory [95].

Focusing the beam not only induces a mixing of the angular momentum components in a beam that carries both spin and angular momenta, but it can also induce the appearance of orbital angular momentum in a beam with only spin angular momentum [114,115], and *vice versa* [116]. For example, an aplanatic lens can be used to focus a circularly polarised Gaussian beam and introduce a phase component of the form $\exp(i\sigma_z\phi)$, which can induce orbital motion of trapped particles [117].

3.5. Rotation in alternative geometries

Going beyond single-beam optical tweezers, many alternative optical trapping geometries have been designed with advantages for particular applications. Rotational motion can also be realised in these alternative geometries. As examples, we consider traps formed by counter-propagating beams, which allow the confinement of larger and motile samples and offer increased resilience to fluctuating experimental parameters [5,118], plasmonic tweezers which allow trapping of very small particles at low optical power [119], and trapping in evanescent fields, e.g. those of optical nanofibres which offer promise for long-range optical trapping within samples [120,121].

3.5.1. Rotation in counter-propagating beams
As in the case of unbalanced scattering and gradient forces in a free-space optical trap, the scattering forces of multiple laser beams, such as two misaligned [122,123] or tilted [124] counter-propagating beams,

can be used to generate a net force able to make the particle follow a trajectory. The speed and shape of the motion can be controlled by the laser power, radial misalignment, axial separation, and angle between the two beams.

Even without imbalanced or misaligned beams, counter-propagating optical traps allow one to have full control over the orientation and rotation of asymmetric particles. This is in contrast to a single Gaussian beam, in which elongated particles smaller than the beam spot tend to align with the polarisation (see Sections 3.1.1 and 4.1.3), while larger particles align their longest dimension along the beam propagation direction [61,113]. In a counter-propagating dual-beam trap, cylindrical particles can adopt a variety of orientations depending on the size, shape, and polarisation of the beams, and the particle's aspect ratio, due to the interplay between the gradient and scattering forces and the generated optical torques [113]. When the counter-propagating beams are linearly polarised along the same direction, a cylinder larger than the beam waist can be stably trapped perpendicularly to the beam axis in one of the high-intensity fringes of the standing wave created by the interference of the beams. A striking example of the utility of rotation in dual-beam traps was provided by Kreysing *et al.* [125], who formed a dual-beam trap using one Gaussian beam and one beam with a dual-lobed transverse profile which could be dynamically rotated. This setup allowed full control of the orientation, and therefore tomographic imaging, of individual cells and cell clusters up to 100 μm in size (Figure 4(a)).

In the balanced dual-beam configuration, if the beams have opposite circular polarisation, the cylinder spins around the beam axis due the transfer of spin angular momentum produced by anisotropic scattering (see Sections 3.1.2 and 4.1.3). This does not happen if the particle is oriented with its symmetry axis parallel to the beam propagation direction [113,126]. In these configurations, rotation can also be produced by orbital angular momentum transfer [113]. A silicon cylinder trapped in the high-intensity ring and parallel to the axis of two counter-propagating Laguerre-Gaussian beams orbits in both linear and circular polarisation. When trapped perpendicularly, both spin and orbital momentum are transferred to the particle, which orbits around the beam propagation direction and spins about its own axis in circularly polarised light (Figure 4(b)). It is worth noting that, if the counter-propagating linearly polarised beams have the same topological charge, the total angular momentum is zero and the particle does not orbit [63].
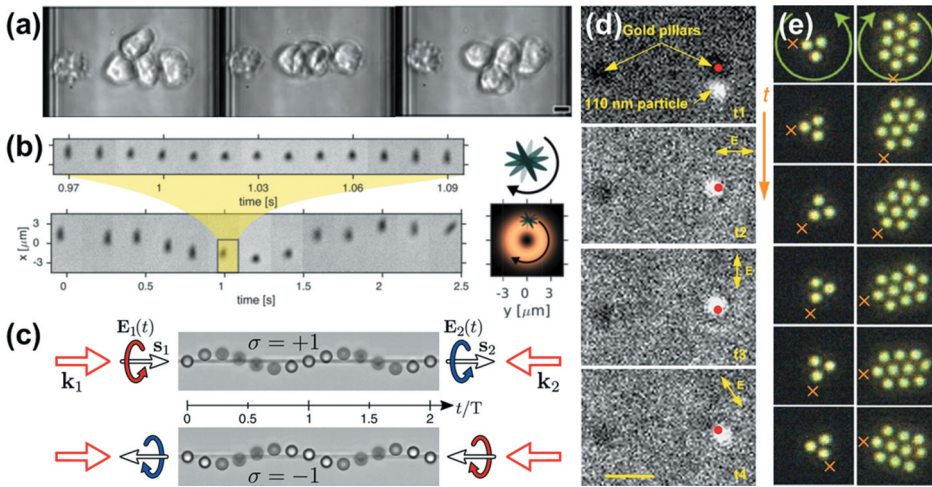
Figure 4. Rotational motion in complex configurations. (a) Rotation of a cluster of cells in a counter-propagating beam trap, where one beam has an asymmetric intensity profile which is rotated. Reprinted with permission from [125] The Optical Society. (b) A silicon nanowire trapped transversely to the beam propagation direction undergoes combined orbital and spinning motion in a circularly polarised trap formed by two counter-propagating Laguerre-Gaussian beams. Adapted with permission from [113]. Copyright 2019 American Chemical Society. (c) A polystyrene microparticle trapped in the evanescent field of a tapered optical fibre follows a helical trajectory. Adapted with permission from [58] The Optical Society. (d) Orbital motion of a polystyrene nanoparticle around a plasmonic nanopillar. The particle is trapped in one of the hot spots generated by the plasmonic tweezer when illuminated with linearly polarised light, and orbits when the polarisation is rotated. Adapted by permission from Springer Nature Customer Service Centre GmbH: Springer Nature, Nat. Commun [56]., 2011). (e) Rotation of two mesoscale optical matter arrays formed by optically bound silver nanoparticles trapped in circularly polarised light. Figure adapted from [138] (CC BY 4.0).

3.5.2. Rotation in plasmonic nanotweezers

Plasmonic nanotweezers are structures able to confine incident light into a sub-wavelength volume. In turn, this enables the creation of enhanced gradient forces able to confine nanoparticles and biological molecules in liquid medium with milliwatts of optical power.[6] Alignment [127] and rotation [56,128,129] of particles can also be achieved in these trapping systems. As an example, Wang *et al.* [56] showed orbiting of polystyrene nanospheres around a plasmonic nanopillar using both linearly and circularly polarised light. When using linearly polarised light, the nanopillar generated two diametrically opposed hot spots at which the particles were trapped. Orbital motion around the pillar was achieved by rotating the linear polarisation (Figure 4(d)). On the other hand, when the plasmonic nanotweezer was illuminated with circularly polarised light, the pillar confined the field in a ring around it with an energy flow in the same direction as the handedness of the light. The particles were trapped in the ring and the scattering force caused them to orbit the pillar in the same

direction as the energy flow. The possibility of introducing rotational motion in nanotweezers widens the application range of rotational dynamics to the nanoscale. These plasmonic structures might be used to fully control the orientation and rotation of untethered biologically relevant single molecules, or to use rotational motion as a battery to store energy from the electromagnetic field [128].

3.5.3. Rotation in optical fibres or resonators

Rotational effects can also be implemented using guided-wave optics such as optical fibres and whispering gallery mode resonators.

Orbital motion of particles driven by light carrying only spin angular momentum can be achieved in the evanescent electromagnetic field produced by total internal reflection and guiding of light, such as in the case of light guided by an optical fibre. In such fields, the spin and orbital angular momenta couple, which leads to the appearance of a spin angular momentum component perpendicular to k. Thus, a particle in that evanescent field can experience a transverse spin-dependent force that can induce orbital motion. This effect was demonstrated by Tkachenko *et al.* [58] using micron-sized polystyrene beads. When two circularly polarised beams with the same polarisation are coupled to opposite ends of a single-mode tapered fibre, the beads follow helical trajectories around it (Figure 4(c)), while orbital motion at a fixed axial position is achieved for balanced, counter-propagating beams with opposite circular polarisation. The authors suggested that, apart from providing very suitable experimental conditions to evidence the existence of a transverse, spin-dependent radiation force in an evanescent electromagnetic field, the rotational dynamics of the particle might have application as a controlled rotary pump to generate fluid fluxes at the microscale.

As another example of rotation in guided light, Arnold *et al.* [59] observed the orbital motion of 375 nm-radius polystyrene nanoparticles trapped in heavy water in the evanescent field created by a circulating whispering gallery mode excited in a 45 μm-diameter silica microsphere. The nanoparticles orbited the resonator at a rate of 0.2 Hz for 40 μW input power, but only for a few revolutions before escaping. The analysis of the dynamics of the particles in the evanescent field was proposed to have applications for mass and size spectrometry.

3.6. Rotation in the presence of multi-particle interactions

So far, we have concentrated on experimental scenarios where we control the rotational motion of individual particles. However, it is possible to simultaneously trap more than one particle, and the rotational motion can be used as a probe of the multiparticle interactions via hydrodynamic

coupling or optical binding. In turn, these can be used to control the rotational motion of more than one particle.

For example, multiple particles can be brought together into a single optical trap by gradient forces and undergo independent rotation (i.e. circulate along a closed trajectory [99,100,130,131]) or rotate as a single entity. In this second situation, the material properties of the individual particles and the total size and shape of the joint structure will determine the applied optical torque. For example, Shen *et al.* [132] confined gold nano-particles in the intensity minimum of a Laguerre-Gaussian beam, and observed the formation of agglomerates of up to three particles. These trimers spun as a single entity in a circularly polarised $\ell = 1$ beam [132], exhibiting the same dynamics as would be seen with a single gold particle of comparable size to the Laguerre-Gaussian ring profile (see Section 3.3). When multiple particles confined within a volume interact with each other, the group of particles may behave differently from a single particle. In fact, it has been widely observed that it is much easier to set a group of particles into rotation than a single one in a highly focused Laguerre–Gaussian beam. Tao *et al.* [133] studied this phenomenon using 3 μm diameter latex spheres in deionised water. The hydrodynamic interaction between the particles leads to a drag torque smaller for the group of particles than that for an individual sphere. The drag on a single particle due to a neighbouring particle depends on their size and relative distance and position. Thus, certain particle arrangements (i.e. a full vs an incomplete ring) can lead to a decrease on the drag torque, leading to a faster rotation. Furthermore, the rotational dynamics of multiple particles circulating in concentric rings constitutes a model for the study of many-body hydro-dynamic coupling at the micron-scale, where the inter-particle interaction occurs within and between rings [131].

In the previous situations, the particles are confined within the high-intensity ring of the Laguerre-Gaussian beam and can act as a whole due to the hydrodynamic interaction. However, the light scattered by each particle, especially in the case of metallic particles, can produce an electromagnetic particle–particle interaction referred to as *optical binding* [134], which makes the particles arrange themselves at a stable position and orientation [113] where the radial forces acting on them are zero. Dienerowitz *et al.* [104] observed the rotation of two 100 nm gold nanoparticles confined to the dark core of a Laguerre-Gaussian beam. The particles underwent syn-chronised co-rotation about the centre of the beam while keeping the largest separation possible. Similarly, multiple dielectric particles trapped in the high-intensity ring of a Laguerre-Gaussian beam orbit around the beam axis at a fixed separation [63].

Apart from controlling the relative position and orientation of the parti-cles, optical binding can give rise to optical torques which result not only in

particles spinning about their own axis under linearly polarised light, but also orbiting together around their common centre-of-mass when trapped in light without orbital angular momentum [135,136]. Haefner et al. [135] theoretically studied the optical torques acting on two optically bound spheres when illuminated by both a linearly and a circularly polarised plane wave. In linearly polarised light, the generated torques produced by conservative forces make the particles orient perpendicularly to the polarisation, as if they were a single, elongated particle (see Section 3.1.1). The particles also spin about their own axis when the dimer is neither parallel nor perpendicular to the polarisation. On the other hand, non-conservative forces generate both orbital and spin torques that set the particles into continuous rotation when illuminated with circularly polarised light. The magnitude of both torques increases with the laser power and particle size, and it will be larger than the thermal-induced motion for certain values of these parameters, thus a priori experimentally accessible. For particles larger than a tenth of the wavelength, the orbital and spin rotation directions change depending on the particle size, and the first is also determined by the relative distance. This is unlike small particles, for which the orbital and spin torques always have opposite direction. They also compare the spin torque due to binding and that produced by absorption for a silica particle and found that the absorption-induced spin dominates for particles larger than one-tenth of the wavelength, but the total optical torque can be below the maximum produced by absorption since the spin torque produced by optical binding can be opposite to the handedness of the polarisation.

These theoretical predictions, in particular the appearance of the a priori counter-intuitive negative optical torque (i.e. rotation opposite to the direction of the beam's angular momentum), were recently experimentally observed by Sule et al. [137] on optically bound dimers formed by 150 nm-diameter silver nanoparticles trapped in deionised water with a focused circularly polarised Gaussian beam. Negative optical torque was only possible for a distance between particles of 400 nm, which was an unstable position, thus hardly accessible in their experimental conditions. At this separation, they observed the transition between the near-field and the optical binding regimes. In the first case (distances of 200–300 nm), when trapped with linearly polarised light, the dimers oriented along[7] and followed the laser polarisation when it was rotated, while under circularly polarised light they rotated around their common centre-of-mass in a direction determined by the handedness of the beam. At optical binding distances ($\sim$ 600 nm), the particles did not rotate in circularly polarised light.

The first realisation of stable and tunable rotation of multiple optically bound particles in a circularly polarised trap was performed by Han et al. [138]. They studied self-organised silver nanoparticles forming mesoscale optical matter arrays with variable number of particles in different

configurations. The particles were trapped against an upper coverslip with a collimated circularly polarised beam and spun around their common centre-of-mass (Figure 4(e)). They experimentally showed that the magnitude and direction of the applied optical torque depended on the number of particles, their separation and configuration. From Mie theory calculations they also found that the lattice plasmon resonance affects the direction of the optical torque, which is negative (i.e. induces opposite-handedness rotation) for wavelengths larger than the plasmon resonance. Their theoretical study and simulations showed that the rotation direction depends on the rotational symmetry of the array and the induced phase retardation. This study enables the design of tunable electro-dynamic materials that allows programmable transduction of light into mechanical forces, and have application as mechanical rotors (Section 5.2) or rheological probes (Section 5.3).

Optical binding can also enhance the interplay between the spin and orbital angular components in circularly polarised Laguerre-Gaussian beams. The azimuthal component of the inter-particle light-induced forces produced by the spin angular momentum can accelerate or decelerate the orbital motion produced by the transfer of orbital angular momentum, as has been theoretically demonstrated by Tamura *et al.* [139].

4. Experimental design

As we have seen in Section 3, the rotational dynamics of the particle depend on its properties and those of the light field. For example, perfectly isotropic non-absorbing spheres experience no torque other than the orbital torque in a Laguerre-Gaussian beam; non-birefringent perfect spheres can spin if they absorb; asymmetric (by birefringence or shape) but non-absorbing particles can spin or librate if they scatter photons. In this section, we discuss the choices available in designing the particle (Section 4.1), the environmental factors which determine the maximum speed of rotational motion (Section 4.2), and review methods for the detection of the particle's rotation and the measurement of the applied optical torque (Section 4.3).

4.1. Making rotors

Tailoring the phase and amplitude of the light allows the generation of orbital motion (Section 3.3). To generate a spin or librational torque usually requires manipulation of the light's polarisation (which can be tuned using waveplates), and the characteristics of the particle. In this section we discuss how the material properties (birefringence, absorption, and shape) of the

optically trapped rotors can be tailored to maximise the transfer of angular momentum and, hence, the rotation rate.

4.1.1. Particles with intrinsic birefringence

A perfectly spherical homogeneous transparent particle will be unaffected by the spin angular momentum of the trapping beam. However, if we provide the particle with an internal asymmetry, i.e. we make the particle with a *birefringent* material, it could rotate around its centre-of-mass due to spin angular momentum transfer.

A birefringent material is one with a susceptibility which is not the same in all spatial directions, i.e. it is not optically homogeneous. When the light passes through such an anisotropic material, the components of the electric field travel at a different speed and therefore undergo different phase shifts, since the material presents different refractive indices along the different spatial directions. As a result, the polarisation of the incident light changes depending on the relative value of the induced phase shifts, leading to a transfer of spin angular momentum.

There are naturally-occurring birefringent materials, such as the calcium carbonate mineral calcite [77] or the silicon oxide mineral quartz [76,140]. The first birefringent particle that was spun in an optical trap was a microscale irregular fragment of crushed calcite (Figure 5(a)) [77]. Although a non-spherical shape can be beneficial for spin angular momentum transfer (see Section 4.1.3), it may complicate the interpretation of rotational motion of the particle seen in experiments, which is mandatory for most applications. For this reason, Bishop *et al.* [141] developed a synthetic method to prepare spherical birefringent vaterite microparticles (Figure 5(b)), another calcium carbonate mineral. Currently, vaterite particles are used for experiments in both the overdamped [46,141–143] and underdamped [144–146] regimes, and even nanovaterite crystals can be synthesised and optically spun [147].

Despite their versatility and widespread use, calcium carbonate minerals (especially of such small sizes) degrade in aqueous media. This motivated the search for novel optically anisotropic materials such as liquid-crystal emulsions [47,148,149] (Figure 5(c)), polymers [70,80] or birefringent synthetic crystals. Micro and nanoparticles made of fluoride crystals, such as $LiYF_4$ (YLF) [83,150] and $NaYF_4$ [17,18,61,151,152] (Figure 5(d)), have also been aligned and spun in optical traps. The main feature of these particles is that the synthesis procedure allows them to be doped with rare-earth ions that provide them with special characteristics such as the ability to control [83,150] and measure [152] temperature. Other types of dielectric particles, such as those made of rutile TiO_2 [153] or Hg_2Cl_2 (Calomel) [101], present higher refractive indices which enhance the applied optical forces and torque.
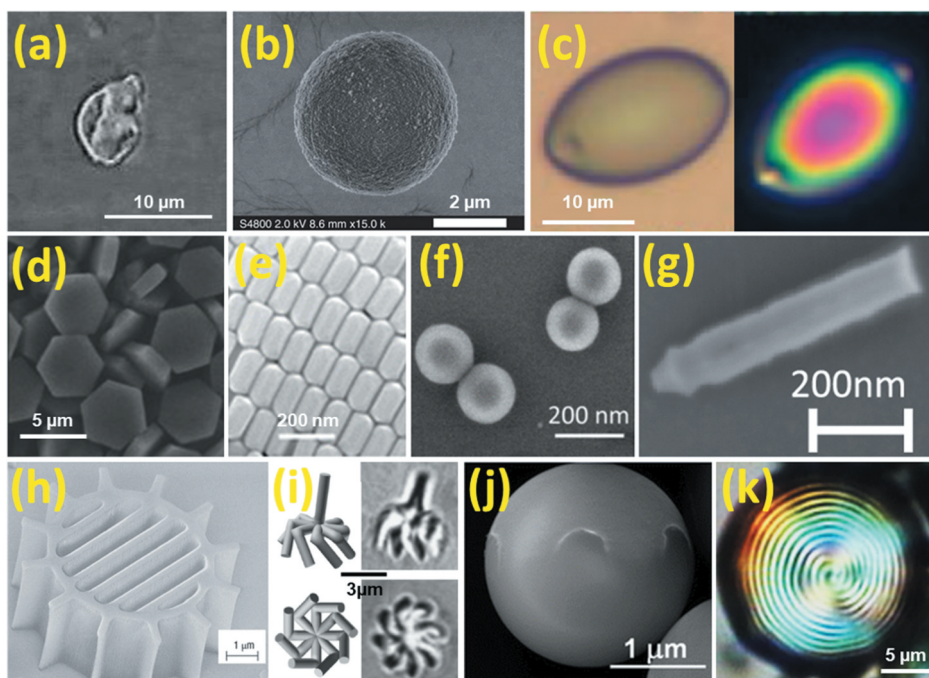
Figure 5. Gallery of rotors. (a) Asymmetric fragment of crushed birefringent calcite (Adapted by permission from Springer Nature Customer Service Centre GmbH: Springer Nature, Nature [77], 1998). (b) Spherical birefringent vaterite microparticle. Figure adapted from [145] (CC BY 3.0). (c) Ellipsoidal birefringent liquid crystal drop. The cross-polarised photomicrograph (right) shows the optical asymmetry of the particle [148] (Copyright 2005 WILEY-VCH Verlag GmbH & Co. KGaA, Weinheim). (d) NaYF$_4$ hexagonal birefringent microdisks [151] (Copyright 2018 WILEY-VCH Verlag GmbH & Co. KGaA, Weinheim). (e) Gold nanorods. Adapted with permission from [92]. Copyright 2015 American Chemical Society. (f) Silica nanodumbbells. Reprinted figure with permission from [81]. Copyright (2018) by the American Physical Society. (g) Silicon nanocylinder. Figure adapted from [82] (CC BY 4.0). (h) Bespoke polymer microrotor. Figure adapted from [158] 2005, Springer Nature. (i) Specially designed resin 'sprinkler'-shaped microrotor for optimised generation of fluid flow. Reprinted from [159], with the permission of AIP Publishing. (j) Janus particle formed by a polystyrene microsphere with a half-shell of gold. Adapted with permission from [169]. Copyright 2015 American Chemical Society. (k) Cross-polarised micrograph of a chiral polymeric spherical birefringent liquid crystal micro-particle showing the internal spiral structure. Figure adapted from [170] (CC BY 4.0).

Quartz, calcite, and vaterite, together with certain crystalline structures and liquid-crystal particles, are *uniaxial* materials, i.e. they present two distinct refractive indices along two orthogonal directions (the ordinary and extraordinary axes). In this case, a birefringence value Δn, given by the difference between the ordinary and the extraordinary refractive indexes ($\Delta n = n_o - n_e$), can be defined. The atomic and crystalline structure of the material determines the particle's birefringence (see Table 1), and the effective value can differ from that reported for the bulk material depending on the illumination conditions (i.e. plane wave/focused beam, portion of the particle's volume that is irradiated).

Table 1. Birefringent particles used in optical rotation experiments.

Material	Δn	Shape	Size (μm)	λ_{laser} (nm)	Ref
Quartz	+ 0.009	Prolate ellipsoid	1	–	[76]
		Cylinder	0.53 × 1.1	1064	[140]
Calcite	− 0.16	Irregular	1	1064	[77]
Vaterite	+ 0.1	Sphere	0.8	532	[147]
			1.5–3.5	1064	[141]
			4.4	1070	[145]
			5	1064	[146]
YLF		Irregular	0.2	~1000	[83]
NaYF$_4$	0.027	Hexagonal disk	5 × 1.2	784	[151]
Rutile TiO$_2$	0.26	Cylinder	0.15–0.4 × 0.5–1.5	1064	[153]
Hg$_2$Cl$_2$	0.683	Irregular	1 × 3	1064	[101]
Liquid-crystal	0.151–0.251	Sphere	1–15	598	[149]
	0.18		0.6–1.2	1064	[47]
	0.14	Spheroid	2	1070	[148]
Fluorinated polyamide	− 0.13	Square	12	1064	[80]
α-eicosene wax		Round disk	2.4	633	[70]

For approximately-spherical particles, size denotes the diameter. For asymmetric particles we use the notation $2a \times d$, where a is the radius, and d the length along the other dimension. We also include the trapping wavelength, as the torque depends on the ratio of particle size to wavelength.

The value of Δn and the size of the particle (i.e. path length of the light travelling through the material) determine the magnitude of the applied optical torque (see Equation 4), since they are responsible for the induced phase shifts in the light polarisation components (i.e. retardation). To optimise the spinning torque (Equation 6) exerted by pure circularly polarised light, the particle should introduce a phase retardation which is an odd-valued integer multiple of π (i.e. the particle should act as a half-wave plate), hence

$$\frac{d}{\lambda_{laser}} \Delta n = \frac{1}{2}.$$ (10)

This means that a particle with a birefringence value in the range 0.01–0.7 should have a thickness of $\sim$ 1–50 times the trapping wavelength to maximise the applied torque.

It is worth noting that the thickness of the particle also determines whether it would rotate under elliptically polarised light [77]. For a given polarisation ellipticity, the particle size can be chosen to produce an orientation torque (first term in Equation 4) weaker than the spinning torque (second term in Equation 4), allowing the particle to always spin even when the polarisation is not purely circular.

4.1.2. Absorptive particles

While only limited materials exhibit birefringence, all materials absorb light to a greater or lesser extent. Dielectric birefringent particles are usually said to be *transparent* since they present weak absorption to

the trapping wavelength (i.e. $\sigma_{\text{scat}} \gg \sigma_{\text{abs}}$); hence, the transfer of angular momentum is dominated by scattering, but not restricted to only it. Nanovaterite particles have been spun in heavy water when trapped with a wavelength of the order or larger than their diameter [147], contrary to what one would expect from the previous discussion in Section 4.1.1. In this case, the spin angular momentum transfer through birefringence was likely complemented by that produced by the absorption of the trapping wavelength.

As we discussed in Sections 3.2 and 3.3, the transfer of both spin and orbital angular momenta can also be achieved through *absorption*. This optical torque (see Equations 7 and 8) is proportional to the amount of laser power absorbed by the trapped particle, which depends on its absorption coefficient. Thus, one can choose to work with particles that present high absorption to the trapping light to enhance the angular momentum transfer and hence the applied optical torque. Unlike dielectrics, the imaginary component of the complex refractive index of metals is significant, which leads to a much larger absorption cross-section (e.g. an $\sigma_{\text{abs}} \sim 10^{-10}$ has been reported for gold nanoparticles in comparison to that for quantum dots $\sigma_{\text{abs}} \sim 10^{-14}$ and dielectric materials $\sigma_{\text{abs}} \sim 10^{-19}$ [154]).

In Table 2 we include examples of particles that have been rotated due to absorption-mediated angular momentum transfer. As can be seen, dielectric particles with low absorption coefficient can be spun but only in vacuum at very low damping rates. Subwavelength particles can also be rotated despite the absorption coefficient decreasing with the particle size. In this situation, one can make the appropriate match between the particle's material and trapping wavelength to take advantage of optical resonances at which absorption is enhanced. The most well-known optical resonances are the localised plasmon resonances that occur in noble metals of nanometric size. The spectral position of these resonances depends on the particle size and shape, therefore these parameters can be tailored to match the experimental requirements.

Table 2. Absorbing particles use in optical rotation experiments.

Material	Shape	Size (µm)	Ref
Gold	Commercial	0.2	[90,95]
CuO	Irregular	1–5	[89]
Silica	Sphere	10	[146]
		0.1	[172]
Graphene	Flake	few	[315]
SiC	Irregular	0.34–16.4	[155]

Size refers to the diameter or longer dimension of the particle. We note that spinning of spherical silica has only been observed in high vacuum due to the extremely low torques applied.

4.1.3. Particles with form birefringence

The particle's *shape* can also be engineered to allow the angular momentum to be transferred through scattering. Non-spherical particles present a *shape-induced birefringence* that will make them experience an optical torque similar to those with an internal birefringence. In fact, the applied torque on an asymmetric particle can be much larger than that exerted on a spherical particle of the same size and made of the same material, leading to faster rotations [49].

Non-spherical particles present a non-homogeneous susceptibility with different values along different spatial directions. As an example, an elongated particle (Figure 5(e-g)) will be more polarisable along its longitudinal direction than its shortest dimension, and this difference can be large enough to allow angular momentum to be transferred even for subwavelength particles or biological material (see Table 3). Hoang *et al.* [75] calculated the susceptibility along the major and minor axes of an ellipsoidal nanodiamond with an aspect ratio of 1.25: χ_x=2.05 and χ_y=1.74, respectively. These susceptibilities give a shape-induced birefringence value of 0.1, comparable to that reported for birefringent crystals (see Table 1).

This shape-induced birefringence can compete with the internal birefringent character of the particle [157]. The dimension that presents the largest susceptibility is referred to as the optical axis of the particle. When trapped in linearly polarised light, the particle will try to align this axis along or perpendicularly to the electric field, depending on the induced light retardation [80]. The symmetry and optical axes of non-spherical birefringent particles are not necessarily the same, as in the case of elongated calcite particles. Thus, these particles present additional rotational degrees of freedom, unlike, for example, quartz particles whose optical and symmetry axes are aligned [76]. The interplay between the susceptibility along these axes

Table 3. Shaped particles used in optical rotation experiments.

Material	Shape	Size (μm)	Ref
Gold	Cylinder	0.065 × 0.130–0.170	[92]
Silica	Dumbbell	0.17 × 0.33	[81]
	Cross	13 × 10	[160]
Silicon	Cylinder	0.13 × 0.725	[82]
		0.078 × 6	[113]
Polystyrene	Oblate ellipsoid	2	[126]
Resin	Sprinkler	10, 5	[159,161]
	Cross	3	[156]
NaYF$_4$	Cylinder	0.14 × 1.1	[61]
Polymer	Bespoke	~5	[158]
Glass	Cylinder	5	[64]
Teflon	Irregular	2	[103]
Chromosome	Cylinder	~6	[64]
Red blood cell	Disk	6	[190]

For approximately spherical particles, size denotes the diameter. For asymmetric particles we use the notation $2a \times d$, where a is the radius, and d the length along the other dimension.

will determine the different torques that act on the birefringent non-spherical particle and its final orientation and rotation axis [17,157].

As discussed in Section 3.1, the potential torques that can be exerted on non-spherical nanoparticles (those with at least one dimension much smaller than the trapping wavelength) can be calculated based on the dipole or Rayleigh-Gans approximations. Within this limit, (which applies to many experimental cases, such as in [49,55,75]) analytic solutions can be found for disks, cylinders [74], and ellipsoids [75]. This allows one to find the spatial asymmetry which gives the largest optical asymmetry (surprisingly, larger aspect ratio does not imply larger susceptibility difference [81]), and hence the maximum optical torque. For the case of non-spherical particles comparable to or larger than the trapping wavelength, the numerical calculation of the exact optical torque is more complex and usually requires the use of numerical methods such as the finite element method [17,126], vector mode solvers [158], and EBCM method [126].

The ability to numerically simulate the optical torque acting on arbitrary shaped particles opens up the possibility of theoretically designing exotic and more efficient optically-driven rotors [158–161] (Figure 5(h,i)). Nowadays, modern synthesis techniques can produce highly monodisperse, uniform particles with tailored size and shape, allowing a high degree of repeatability and predictability in the experiments. The development of microfabrication techniques, such as reactive ion-beam etching [160], photo- [80,162] and electron-beam lithography [158], or photo-polymerisation [45,159,161,163], has enabled the production of particles of almost any shape in a wide range of sizes. In this case, the particles are made of materials, such as resins and polymers (photoresist), which only interact with the laser angular momentum through their shape. In contrast, the available particle shapes for birefringent [164,165] or metallic [166] particles, which are usually produced by wet chemical synthetic methods, are limited to those allowed by the atomic structure of the crystal (i.e. sphere, cylinder, disk, cube). This can be controlled through the reaction conditions and reagent concentrations. Finally, another simpler strategy to produce non-spherical entities to which angular momentum can be transferred is sticking together multiple beads [81,167] (Figure 5(f)).

4.1.4. Exotic rotors

Theoretical modelling also leads to the design of even more exotic hybrid particles composed of two or more parts that differ in their physical and chemical properties: the so-called Janus particles [168]. As an example, hybrid particles formed by a polystyrene sphere with a half-shell of gold have been shown to undergo stable rotation under linearly polarised light [169] (Figure 5(j)).

Despite the potential of theoretically devising novel light-driven rotors, care must be taken when designing the particle because the parameters should be within the experimental capabilities, i.e. the particle's characteristics that lead to the maximum angular momentum transfer may hamper the optical confinement of the particle within the trap. This is the case of, for example, chiral polymeric liquid crystal particles formed by molecules arranged in such a way that they can selectively reflect light with the same helicity as their internal structure (Figure 5(k)), through a Bragg reflection process [170]. As the transmitted light changes its angular momentum, the particle experiences an optical torque which will be maximum when the handedness of the light matches the helicity of the particle. However, in these high-reflection conditions, the particle will not be confined in the optical trap, but propelled in the beam propagation direction. The reflection efficiency depends on the wavelength and the particle size, thus these parameters should be carefully selected to allow both trapping and rotation.[8]

4.1.5. Multi-particle rotors

While asymmetric particles can be produced by sticking together two beads, multiple particles do not need to be physically attached to act as a single entity. Optically bound particles can form so-called *mesoscale optical matter* [138] (Figure 4(e)), which can undergo interesting rotational dynamics due to the inter-particle interactions, as discussed in Section 3.6. In fact, the rotational dynamics of the assembly of particles that behave as a whole can be controlled by the constituent particles' characteristics (size, shape and material), the separation between them, and the geometry and symmetry of the array.

4.2. Maximum rotation rate

While care may be taken in the choice of particle and the polarisation, topological charge and power of the trapping light to produce the largest possible optical torque, the maximum rotation rate is also governed by the properties of the environment.

Independently of the origin of the optical torque τ_{opt} that drives the rotation of the trapped particle, when it moves inside a medium, a drag torque τ_{drag} will appear counteracting τ_{opt}. This drag torque depends on the properties of the particle (size, shape) and the surrounding medium (viscosity, pressure, temperature), through the rotational drag coefficient γ_{rot}. The magnitude of τ_{drag} is linearly proportional to the rotation rate of the particle in the low Reynolds number regime (which is the case for all particle sizes and experimentally achieved rotation rates in both liquid and gas). As

an example, the rotational drag coefficient of a sphere spinning far from any surfaces in a fluid with a viscosity η is $\tau_{\mathrm{drag}} = 8\pi\eta a^3 \omega_{\mathrm{rot}}$.

As we have explained in Section 3.1.1, the librational motion of a particle trapped in liquid medium is driven by the thermal-induced Brownian motion, which depends on temperature. In addition, the particle angular motion is restricted by the viscosity of the surrounding medium, i.e. the mean square angular displacement $\langle \Delta\theta^2 \rangle$ of the librational particle in a low-viscosity medium would increase more rapidly than when it moves in a high viscosity medium since $\langle \Delta\theta^2 \rangle = \frac{2k_{\mathrm{B}}T_{\mathrm{env}}}{\gamma_{\mathrm{rot}}} t$ [70]. This is only the case for short times $(t \ll \gamma_{\mathrm{rot}}/\kappa_\theta)$, when diffusion dominates, while for long times $(t \gg \gamma_{\mathrm{rot}}/\kappa_\theta)$ the particle displacement is restricted by the applied torque, i.e. $\langle \Delta\theta^2 \rangle = \frac{2k_{\mathrm{B}}T_{\mathrm{env}}}{\kappa_\theta}$. This dependence of the librational displacement on the viscosity of the surrounding medium has application in the characterisation of the rheometric properties of liquids (see Section 5.3).

In the underdamped regime the librational frequency is independent of the properties of the environment (viscosity, pressure or temperature) but the coherence of the oscillations increases as the gas damping decreases, giving rise to high-Q oscillators [75,83]. This allows the properties of the environment to be measured from the librational damping [83], in analogy to environmental sensing with translation.

The dynamics of spinning particles offers an interesting departure from the harmonic oscillator physics of the librational motion. In this case, the maximum rotation frequency $\omega_{\mathrm{rot}}^{\mathrm{max}}$, which is given by the balance between τ_{opt} and τ_{drag}, is inversely proportional to the drag coefficient $\gamma_{\mathrm{rot}} = I\Gamma_{\mathrm{rot}}$ in both over and underdamped regimes

$$\omega_{\mathrm{rot}}^{\mathrm{max}} = \frac{\tau_{\mathrm{opt}}}{I\Gamma_{\mathrm{rot}}}, \tag{11}$$

where I is the moment of inertia of the particle and Γ_{rot} the rotational damping rate. The maximum rotation rate can be set experimentally by tuning τ_{opt} (see Sections 3.1.2 and 3.2); hence, the spinning particle can act as a light-driven actuator (see Section 5.2) able to apply a controlled stress, which is especially relevant for rheometric studies (see Section 5.3).

The maximum rotation rate will also be determined by γ_{rot}, which depends on the orientation of the particle in respect to the rotation axis (through I); on the mass, volume and shape of the particle[9]; and also on the properties of the environment, i.e. viscosity/pressure [82,145] and temperature [152]. In analogy to the translational motion (see Equations 2 and 3), the rotational damping rate for a spherical particle $(I = 2/5Ma^2)$ spinning at low pressure $(\hat{l} \gg a)$ is given by

$$\Gamma_{\text{rot}}{}^{\text{Kn} \gg 1} = 12.38 \frac{a^2}{M} \sqrt{\frac{2\pi M_{\text{gas}}}{k_B T_{\text{env}}}} P_{\text{gas}}. \tag{12}$$

This equation only holds for spherical particles. For asymmetric particles, a similar expression can be found with the same dependence on the environmental properties and a proportionality constant that depends on the geometry of the particle [171].

This damping rate limits the maximum rotation rate that can be achieved for a given applied optical torque. For example, microparticles in water have been reported to spin at hundreds of Hz [141], while nanoparticles can rotate at tens of kHz [92,147] in liquid media due to their reduced size. If the particle is trapped in a medium with a lower viscosity such as air, faster rotations can be generated. In fact, in low pressure, spinning particles have been recorded as the fastest man-made spinning objects [49,81,145,172] with rotation speeds as high as 5 GHz achieved for a nanodumbbell [49] in vacuum. It is remarkable to note that, in the space of just over two decades, the state-of-the-art rotation rate achieved by spin angular momentum transfer has advanced by over seven orders of magnitude, from a few hundred Hertz [77] to 5 GHz [49].

As pressures approach the ultra-high vacuum range (typically $< 10^{-6}$ mbar), the drag produced by the surrounding molecules is negligible and the rotation rate of levitated nanoparticles is limited only by the material properties of the particle [50,81,172–175]: eventually the centrifugal force acting on the particle will cause it to be ripped apart. Thus rotational motion provides an interesting new platform to test the material properties of the particle under extreme conditions. For example, at GHz rotational rates, the maximum stress exerted on a 170 nm-diameter nanodumbbell was found to be 13 GPa [81], two orders of magnitude larger than the ultimate tensile strength of bulk glass.

The exceptionally low values of γ_{rot} in low viscosity environments even allow transparent isotropic particles, such as silica beads, to undergo rotation at high frequencies [146,172]. Monteiro *et al.* [146] reported MHz rotation rates for 10 μm diameter amorphous silica spheres, which were driven by the weak torque likely produced by transfer of spin angular momentum through the residual absorption of the trapping laser.

The same way as τ_{drag} places a ceiling to the maximum speed achievable by a spinning particle, the $\omega_{\text{rot}}^{\text{max}}$ of an orbiting particle is determined by τ_{opt} and γ_{rot}. In this case, the drag coefficient is proportional to the linear velocity, i.e. $\gamma_{\text{rot}} = \gamma_q = 6\pi a \eta$ (see Section 2), and $\tau_{\text{drag}} = 6\pi a \eta r_\ell \omega_{\text{rot}}$ is dependent of the trajectory radius r_ℓ [95].

However, in low-pressure environments, it was shown that (unlike the spin or libration frequency) the maximum orbital rotation frequency of

a silica microsphere in a Laguerre-Gaussian beam was limited by the optical trapping forces [176]. More specifically, the inertial forces must not be larger than the restoring force of the trap, which is equivalent to stating that the rotation rate can be no higher than the radial trap frequency (assuming circular symmetry). Svak *et al.* showed similar trap-ejection phenomena due to chaotic orbital motion of a silica microsphere in a circularly polarised Gaussian trap [177]. For more complex beams, more intricate orbital trajectories can be realised in spite of these ejection effects. In Ref [178]., Arita *et al.* demonstrated an optical trap generated by a Bessel beam, which formed a 'perfect' vortex[10] annulus at the focal plane. In this focal plane, orbital angular momentum was transferred to a silica microsphere, which underwent orbital acceleration until it overcame the restoring force of the trap. However, due to the change in the beam profile along its propagation direction, the particle was recollected and returned to the bright annulus, forming complex trajectories in a closed three-dimensional loop.

4.3. Detection of rotation and optical torque

As we will explain in Section 5, the use of the rotating particle for any application requires the accurate experimental determination of the rotation rate and the applied optical torque.

The rotational dynamics of the particle can be monitored using a camera with sufficient spatial and temporal resolution. This simple method can be used for any material particle and it is especially useful to characterise the orbital motion. To be applied for spinning particles, they must show an asymmetry in the plane captured by the camera. In all cases, the size of the particle should be well above the diffraction limit, but the detection of small scattering particles (e.g. metallic nanoparticles) can be facilitated using dark-field illumination [92]. If the frame rate is not high enough to give a reliable measure of the rotation rate, techniques such as stroboscopic illumination [145] or post-processing analysis of the images, can be used to increase the temporal resolution.

The limitations imposed by cameras in the measurement of the fast rotation rate of highly spherical or small particles can be overcome making use of fast photodetectors. In this case, the dynamics are imaged using the changes produced by the particle on the intensity or polarisation of a reference laser beam, which can be the trapping laser itself or an auxiliary detection beam. For the detection of spinning motion, the irregularities of the particle produce a change in the intensity of the forward and back-scattered light depending on the particle orientation, which is monitored in the detector [90]. For birefringent particles, the polarisation modulation of the beam produced by the particle can be converted into intensity changes using polarising elements (e.g. a polarising beam splitter) [145]. The

combination of different detectors can enhance the detection of highly symmetric particles [75,141]. To detect librational motion, where the absolute change in polarisation can be small, it is advantageous to measure both beams emanating from the polarising beam splitter on a balanced photo-detector pair [81]. The orbital rotation rate can also be acquired by a photodetector by the use of a pinhole which only allows the forward scattered light to reach the detector when the particle passes over it [101]. In all cases, the rotational motion of the particle will be evidenced in the photodetector signal as a periodic modulation. The rotation rate can be obtained from the Fourier transform of the signal (more specifically, the power spectral density is commonly used), which would display peaks at the rotation rate or the double of its value (for spinning particles), and at its harmonics [145]. Alternatively, the rotation frequency can be read off as the inverse of the time elapsed between two peaks in the autocorrelation function of the signal [90].

The rotation of the particle can also be monitored via the rotational Doppler effect [179]. Finally, the spectral shape of the emission of certain types of luminescent particles is orientation-dependent and can therefore also be used to track the rotational motion [18,61].

The measured rotation rate of the particle links the applied optical torque with the drag coefficient (Equation 11). If this drag coefficient is known, the optical torque can be directly determined from the measurement of the rotation rate. However, in most applications, the properties of the environment, i.e. viscosity (Section 5.3) or temperature (Section 5.4), are those to be determined, and in this case the optical torque must be experimentally measured. How this can be done depends on the origin of the optical torque. For particles spinning due to the transfer of spin angular momentum through absorption (Section 3.2), the optical torque is proportional to the fraction of the laser power that is absorbed by the particle (Equation 7), and the optical torque is determined from the difference in power of the beam before and after it passes through the particle.

In the case of asymmetric non-absorbing particles (Section 3.1), the optical torque is proportional to the laser power P_{laser} and the change produced in the polarisation of the light $\Delta\sigma$ when it passes through the particle, i.e. $\tau_{opt} = \Delta\sigma P_{laser}/\omega_{laser}$. Knowing the laser wavelength and power, only $\Delta\sigma$ must be experimentally determined. The polarisation coefficient $\sigma = (P_L - P_R)/\sigma_z$ of a light beam can be measured using a polarimeter composed by a half or quarter waveplate and a polarising beamsplitter, which splits the left P_L and right P_R polarisation components. The power of each of these is measured on separate photodetectors [78,180]. The difference between the polarisation coefficient of the beam before and after it passes through the

spinning particle gives the change produced in the polarisation of the beam $\Delta\sigma = \sigma_{in} - \sigma_{out}$.

In torsion balance experiments, the particle is forced to maintain a constant alignment thanks to the orientation torque (Section 3.1.1). In this situation, the applied optical torque is proportional to the angular displacement from this stable orientation produced by rotational Brownian fluctuations or any external force or torque. Thus, as for a particle undergoing translational Brownian motion where the trap stiffness can be retrieved from the position distribution, the angular position distribution $<\Delta\theta^2>$ is used to determine the optical torque $\tau_{opt} = \kappa_\theta\theta$, with $\kappa_\theta = 2k_B T_{env}/<\Delta\theta^2>$ (see Section 4.2). In addition, the optical torque can be calibrated against a known applied torque or force that displaces the particle from its stable orientation.

The resolutions of torque measurement and angular confinement are limited by the rotational Brownian motion of the particle [76]. A particle trapped in a strong optical trap and subjected to a weak torque may display no rotational motion. Surprisingly, in this situation, the tiny optical torque can still be retrieved from the translational Brownian dynamics of the particle [181]. The transfer of angular momentum to the particle induces an imperceptible rotational motion, but this induces a coupling of the in-plane translational modes of oscillation of the particle. The presence of this coupling can be detected in the auto- and cross-correlation functions of the position distribution and the optical torque can be retrieved from the mean square displacement of the particle.

5. Applications of rotational motion

Now, we turn our attention to areas of application for rotating particles. We will review some of the key current and future examples where rotational dynamics offer significant advantages over other platforms or over the translational motion.

As we have seen, the properties of the particle can be tailored (see Section 4.1) to enhance its interaction with the light field, which can be used to reveal hidden properties of the light through the induced rotation of the particle (Section 5.1). Moreover, the rotating particle also actively interacts with its surroundings, e.g. creating fluid fluxes, therefore it can be used as a tiny but powerful actuator (Section 5.2) to apply forces or trigger processes at the microscale. This fundamental relationship between the rotational dynamics and the surrounding medium (see section 4.2) makes rotating particles ideal probes to infer changes or measure absolute values of the properties of the environment (Sections 5.3 and 5.4) or the particle itself.

Optically trapped particles are a powerful platform for precision force and torque sensing (Section 5.5), with important discoveries already realised in the overdamped regime such as measurements of the torques produced by small molecular motors that form part of the intricate internal machinery of the cell. In the underdamped regime, they promise to shed light on important questions in fundamental physics: putting test particles into rotation promises to enhance the sensitivity of levitated particles to hitherto unobserved short-range forces related to the presence of dark matter, dark energy and vacuum-induced friction. Finally, we will discuss proposals and prospects for the realisation of macroscopic quantum objects in rotation (Section 5.6), which may offer insight into the boundary between quantum and classical physics.

5.1. *Measuring and manipulating properties of the light*

As discussed in Sections 3.4 and 3.5, the mechanism for the rotation of the particle can depart from the simple cases of spinning in polarised light and orbital motion produced by light beams with orbital angular momentum. The phenomena that give rise to these rotational dynamics are linked to special properties of the light field and light-induced effects. Thus, the rotating particle can be used as a powerful probe of the properties of non-trivial light fields [58,101,178,182], where the particle is not only sensitive to the linear but also the angular momentum of light. As an example, the transfer of both spin and orbital angular momentum to a birefringent particle can be used to determine the radial evolution of the local intensity of a circularly polarised high-order Bessel beam. The intensity profile of this beam comprises a number of concentric rings with increasing radius r_ℓ and the same energy, thus the local intensity is inversely proportional to r_ℓ. As the spinning torque is directly proportional to the local intensity of the beam, the spinning rate is expected to decrease as $1/r_\ell$. On the other hand, the azimuthal force that leads to the orbital motion of the particle is proportional to the local intensity and inversely proportional to the square of the ring radius, thus the orbiting rate should go as $1/r_\ell^3$. Garcés-Chávez *et al.* [101] confirmed this theoretical prediction by measuring simultaneously the spinning and orbiting rates of a mercury chloride birefringent particle trapped in different rings of the beam, evidencing that both the local intensity and local angular momentum density of the beam can be measured *in situ*.

Interestingly, the rotating particle can also be used to observe 'virtual' properties of the light [177,182] or determine their nature, such as the intrinsic or extrinsic character of the spin and orbital angular momenta [97]; demonstrate the mechanical action of conservative and non-conservative optical forces [69] or the spin flow of a light field [183]; study

how light interacts with matter [98]; and evidence spin-orbit interactions [58,99,117,184,185] or other phenomena such as the spin Hall shift [184]. Moreover, the high rotation rates achieved by spinning particles in vacuum are increasing prospects for the observation of Zel'Dovich amplification of electromagnetic waves [186,187].

5.2. Micromachines

New microfabrication techniques have made possible the miniaturisation of a variety of devices. One of the fields that has benefited from this is the area of microfluidics, where small volumes of liquid need to be precisely controlled. This requires the remote control of microcomponents able to pump, mix and move liquids at the microscale [188,189], enabling near-field hydrodynamic micromanipulation, which allows spatial control of objects without direct contact from the laser beam. One of the simplest yet more powerful ways to do that is making use of the shear flow produced by a rotating microparticle.

Classical hydrodynamic theory can be used to analytically model the fluid velocity $v(r)$ around a sphere spinning within a Newtonian fluid, with a magnitude proportional to the sphere radius and decreasing with the square of the distance r from the sphere centre[142]

$$v(r) = \omega_{\mathrm{rot}} \frac{a^3}{r^2}.$$ (13)

In this case, the flow has a circular symmetry around the particle and its velocity and direction can be easily controlled by simply adjusting the rotation rate and direction of the micro-pump through the applied optical torque. The fluid velocity can be measured by tracking a probe particle which is free to move in the generated flow [142]. The measured extension of the fluid flow generated by a 1.8 µm radius vaterite vaterite particle rotating at 13.4 Hz is shown in Figure 6(a). As can be seen, the fluid velocity rapidly decreases to 15% of the particle rotation rate at a distance from the particle surface equal to it radius.

A directional linear flow along a microchannel can be produced by two adjacent counter-spinning vaterite microparticles [143]. Li *et al.* [190] created a biocompatible microactuator by trapping an array of spinning red blood cells along a line trap formed by two counter-propagating beams. The chain of red blood cells was aligned transversely to the microfluidic capillary and transported microparticles along the channel thanks to the generated local flow. Despite some experimental limitations, they were able to assemble the microactuator inside a living zebra fish, showing the potential of biocompatible light-driven rotors. Vortex flows in the medium can be generated by particles orbiting around a circular trajectory. Zou *et al.* [60] used a scanning
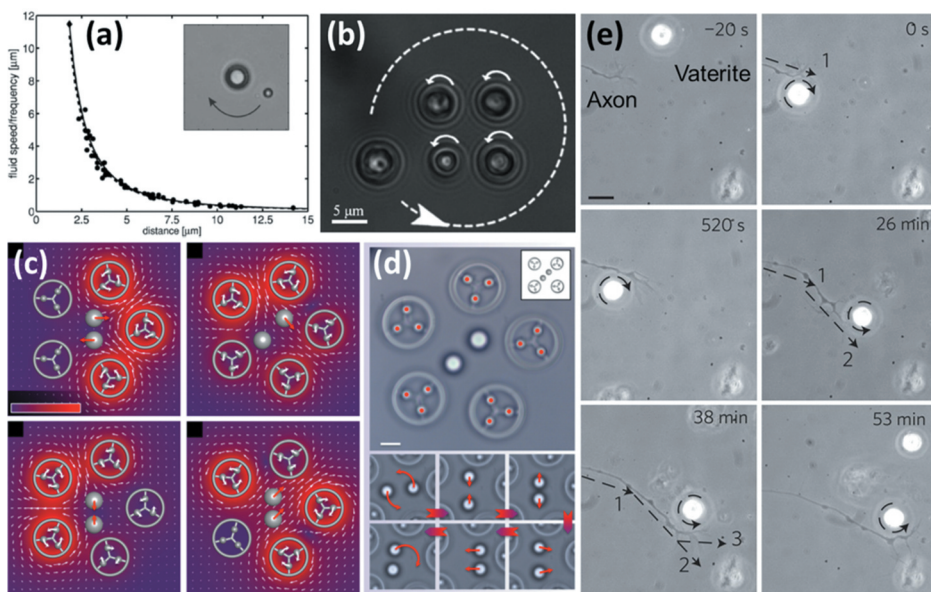
Figure 6. Optically rotated micromachines. (a) Velocity flow generated by a 1.8 μm vaterite particle as a function of the distance from the particle centre (measured by a probe particle as shown in the inset). Reprinted figure with permission from [142]. Copyright (2005) by the American Physical Society. (b) An orbiting trapped cell generates a fluid vortex which spins the four untrapped cells contained within the orbit. Figure from [60]. Copyright 2020 WILEY-VCH Verlag GmbH & Co. KGaA, Weinheim. (c-d) Independent motion of two target spheres driven by the optical manipulation of five custom-made rotors. Figure taken from [45] (CC BY 4.0) (e) By repositioning and spinning a trapped vaterite microsphere in close proximity to an axon, the axon growth direction is controlled (Adapted by permission from Springer Nature Customer Service Centre GmbH: Springer Nature, Nature Photonics [46], 2012).

optical tweezers setup to drive particles and cells along a circular trajectory, within which a microvortex was created which was able to spin multiple cells simultaneously (Figure 6(b)). In this case, the orbiting motion of a single rotor is converted into spinning motion of the targeted entities, which would be very difficult to accomplish using spinning rotors or other means. However, the complementary process is possible: multiple independent spinning rotors can be used to precisely transport target particles along complex trajectories that depart from the simple directional motion along a microchannel. Būtaitė et al. [45] used custom laser-written microrotors to precisely control the positions of multiple target particles along arbitrary trajectories using fluid forces alone. They used a real-time feedback loop to actively change the rotation rate and position of up to 5 actuators for a precise control of the target particles whose positions were continuously monitored (Figure 6(c,d)). They suggested that this high level of control could be applied for the investigation of femtonewton-scale cell–cell interactions in a minimally invasive manner. Laser-driven microrotors have even been used to trigger and study cellular processes: Wu et al. [46] showed that the microfluidic flow

generated by an optically rotated vaterite microcrystal can be used to drive the growth of individual axons (Figure 6(e)).

Beyond the induction of fluid flow, the conversion of heat into useful mechanical motion is a long-standing area of study in physics and engineering and, as in many areas of engineering, there is a continual drive to make technology smaller and more efficient. For rotors trapped in liquid, thermal energy can be converted into rotational motion as the local heating of the medium increases the rotational speed of the particle due to the decrease of the viscosity [90,147,151] (see Sections 4.2 and 5.4). In addition, photothermally induced convection currents can be harnessed to produce rotation and circulation of particles suspended in liquid media [191]. Devices are now being realised in regimes where quantum physics becomes increasingly important, driving much research into quantum thermal-absorption machines [192–195]. Optically trapped particles in vacuum provide a powerful tool to investigate thermodynamics at the nano- and microscale, as reviewed in [196]. Particularly, optically trapped thermally excited rotors offer an analogy to pistons, converting input energy into rotational motion.

The spin motion of optically levitated nanorods in vacuum has been considered as a promising platform for an efficient autonomous heat engine, both in the classical and quantum regimes [197], where the disordered energy of a thermal bath can be converted and stored in the rotational mode of the nanorod without any need for external control to extract the work. In a recent alternative scheme, Arita *et al.* showed that the random thermal fluctuations of background gas can be harnessed to generate coherent oscillations of an optically levitated birefringent microsphere in a linearly polarised beam [198]. Non-conservative coupling between the rotational and translational modes of motion [177,199] results in rotation around the axis orthogonal to both the beam polarisation and the propagation axis, synchronised with translational motion along the direction of polarisation. This coupled motion displays exceptionally high mechanical quality factors above 10^8.

Already, the construction of complex quantum machines is being considered. Liu *et al.* theoretically investigated the dynamics of coherently coupled quantum rotors as an elementary gear [200]. While the optical binding of two trapped microspheres in vacuum was demonstrated in [201,202], the coupled dynamics of nanoscale rotors has not yet been demonstrated experimentally.

5.3. Microrheology

There is an increasing interest in the understanding of rheological properties such as viscosity, elasticity or creep compliance of fluids at the

microscale, which cannot be accomplished with commercial macroscopic linear and rotational viscometers. The field of microrheology has become more important since it has been proven that the bulk properties of complex liquids (e.g. polymer solutions [142] or intracellular medium [17]) differ from those measured at the microscale [142,203]. These microscale properties are those which affect the motion, diffusion and interaction of small molecules that play an important role in many biological processes and chemical reactions. Moreover, in some circumstances, such as in clinical tests, the amount of liquid to be handled is limited, necessitating a capability to study volumes as small as picolitres.

The basic microrheometric techniques are based on the analysis of the translational Brownian motion of a probe particle moving through the medium along a random trajectory [204]. The mean square displacement of the particle is tracked and then related to the viscosity of the medium through a diffusion equation. Optically confining the particle in the desired location allows one to perform targeted, localised measurements of the fluid properties [205,206]. Then, the viscosity can be measured from the harmonic motion of the centre-of-mass of the particle inside the optical trap. Despite their simplicity, since they are just based on tracking the particle displacement, *passive* methods lack the capability of applying a controlled stress or stimuli to study the reaction of the fluid, which is of great interest in the understanding of the behaviour of viscoelastic fluids that would behave as viscous-like fluids or would present elastic-like properties depending on the speed and amplitude of the particle motion [204].

To overcome this limitation, many *active* microrheometric techniques have been developed using optically trapped particles [207]. In this case, the particle is optically forced to translate within the fluid. This produces a shear rate which depends on the velocity of the particle. Even though optical trapping allows one to perform very small displacements, the required translational motion would hinder highly localised measurements of properties near other surfaces.

In this regard, the rotational degree of freedom provides an advantage. A spinning particle applies a shear rate to the surrounding medium that is in close proximity to its surface without the need of any displacement of its centre-of-mass (see Section 5.2 and Figure 6(a)). This tighter confinement of the flow compared to methods based on translational motion ensures a smaller volume is probed [16]. As an example, Knöner *et al.* [142] studied the rotation of vaterite microparticles inside a non-Newtonian fluid formed by a polymer solution. They detected the presence of a depletion layer of less than 100 nm width at the surface of the rotating particle caused by the reduction of the number of polymer molecules, which reduced the apparent viscosity affecting the rotational dynamics of the particle.
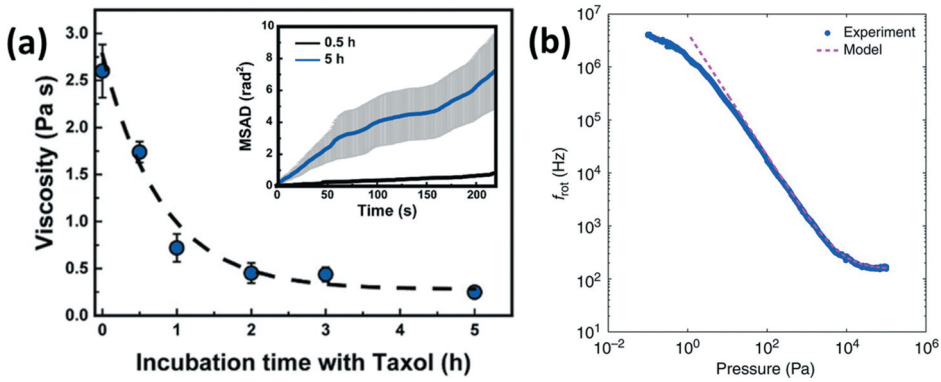
Figure 7. Microrheology and pressure measurement with rotating particles. (a) Intracellular viscosity measured for cancerous cells incubated with the anticancerous drug Taxol, as a function of the duration of the treatment. Inset: the viscosity is retrieved from the evolution of the mean square angular displacement (MSAD) of a librational particle located inside the cell [18] (Copyright 2019 WILEY-VCH Verlag GmbH & Co. KGaA, Weinheim). (b) The rotational frequency of a vaterite microsphere as a function of the environmental pressure. As the rotational damping rate decreases, the maximum rotation rate increases as a result of the balance between the optical and drag torque. Figure adapted from [145] (CC BY 3.0).

The magnitude of the applied stress is directly related to the rotation rate of the particle, which can be controlled through the optical torque, and measured (see Section 4.3) for the characterisation of the fluid properties. Different passive and active microrheometric techniques have been developed based on the application of an optical torque to a trapped object.

Passive techniques take advantage of the librational motion (Section 3.1.1) of the particle. As we explain in Section 4.2, the evolution of the mean square angular displacement of the particle depends on the viscosity of the surrounding medium. For example, the librational motion of asymmetric $NaYF_4$ birefringent particles has been used to determine the changes produced in the intracellular viscosity of cancerous cells treated with anti-cancerous drugs, which affected the internal structure of the cells [18]: the intracellular viscosity was reduced by 85% when the incubation time with the drug Taxol was increased from 0.5 to 5 h (Figure 7(a)), which was determined from the increase in the rate at which the mean square angular displacement of the librational particle evolved with time (inset in Figure 7(a)).

Regarding active techniques, an optically rotated particle can be used as a *microviscometer* to measure the viscosity of the environment [17,141,142,144]. As explained in Section 4.2, the spinning particle will achieve a terminal velocity ω_{rot}^{max} given by the balance between the optical and the drag torques (Equation 11). Therefore, the drag torque, and hence the viscosity of the surrounding medium, can be obtained from the

measurement of the rotation rate of the particle and the applied optical torque (see Section 4.3).

For the method to give an accurate measurement, the drag coefficient must be well known. For this reason, spherical particles [16,141,142,144] are the most suitable probe particles since the drag coefficient has a simple analytical expression, though non-spherical particles [17] have also been used. The asymmetric particle can be approximated to a sphere with an effective radius related to the actual particle surface and volume, or an expression for geometrical shapes (i.e. spheroid [70,126,208], disk [77], cylinder [113]) can be used, but accurate determination of the viscosity requires the modelling of the drag torque for more exotic non-spherical particles [209], the same way as the applied optical torque (see Section 4.1.3).

In addition to a precise determination of the applied torque, laser power and the particle's properties, other phenomena may contribute to erroneous viscosity determination. It is well known that viscosity depends on temperature. Laser-induced heating due to absorption, or less-frequently anti-Stokes laser cooling [150,210], of the particle can change the medium's temperature by conduction (see Section 5.4) and must therefore be carefully accounted for in extracting the viscosity. In 2007, Perkin *et al.* made a detailed study of a vaterite-based microviscometer, including polarisation instabilities and laser-induced heating, which generated a non-uniform temperature gradient in the medium surrounding the particle. They showed that, once the viscometer was perfectly characterised (i.e. all effects considered), it could be used to determine the viscosity, with 10–15 % statistical accuracy, of picolitre volumes of eye fluid and inside a laser-induced cellular protrusion.

Apart from thermal effects, the nature of the fluid under study must be considered. In most cases, the particle is embedded in a viscous medium (e.g. water or air). However, rotating particles also have application in the characterisation of complex fluids at the microscale [17,142], where other factors such as the dependence of the viscosity on the particle's size [203] and rotation rate (i.e. shear rate [207]) must be taken into account.

Finally, the presence of boundaries or nearby particles (see Section 3.6) affects the dynamics of the rotating particle [141,144]. In particular, the drag coefficient increases when the particle rotates in close proximity to a surface [73], which must be considered to avoid underestimating the applied optical torque when determined from the drag torque.

In gaseous environments, similar viscosity measurements can be performed. For example, Arita *et al.* extracted the viscosity of picolitre volumes of air, CO_2 and Ar using optically levitated rotating vaterite microspheres [144]. These sensors can also be used as non-ionising residual gas analysers to measure the composition of a gaseous environment: the drag depends on

the momentum exchange between the trapped particle and the gas molecules, and therefore the molecular mass of the gas [144,211].

In lower pressure environments, attention often shifts from viscosity to pressure. When the mean free path of the gas is much larger than the size of the trapped particle, the rotational drag coefficient varies linearly with the pressure (Equation 12) and the maximum rotation rate of the particle is inversely proportional to pressure (Figure 7(b)). Measurement of pressure via the torsional drag on a rotor was an idea originally proposed by James Clerk Maxwell [212], and is today commonly performed with magnetically levitated mm-scale stainless steel spheres. These spinning-rotor gauges offer attractive features of probing the pressure in the immediate vicinity of the particle, and unlike other types of gauges do not perturb the environment they are measuring via thermal or ionisation effects.

Optically levitated spinning nano- and micro-particles can be used as miniaturised spinning-rotor vacuum gauges. Blakemore *et al.* spin 5 μm-diameter silica microspheres using electrostatic forces, which can be switched off to remove the driving torque [211]. After the switch-off, the rotation rate decays exponentially with a time constant I/γ_{rot} and is therefore inversely proportional to the pressure in the vicinity of the microsphere. The method allows the extraction of pressures with a precision of 7%, across a range from $10^{-6} - 10^{-3}$ mbar, with a measurement time of around 10 s.

A faster method to extract pressure can be accomplished with optically levitated particles undergoing a driven rotation, where there is direct access to the drive signal. Such a scenario can be accomplished by fast-switching between linear and circular polarisation such that the particle's motion is frequency-locked to the drive [213], or by driving the rotation through interactions between the particle electric dipole moment and a rotating electrostatic field [211,214]. Access to the drive signal allows the measurement of the phase lag between drive and particle rotation. This is sensitive to many properties of the environment, including the rotational damping coefficient, and the magnitude of the drive torque. Kuhn *et al.* measured the phase lag of a silicon nanorod's rotation in a standing-wave optical trap to determine pressure over a narrow range of 4–10 mbar but with a precision of 0.3% [213]. For the electrostatically driven silica microsphere of Blakemore *et al.*, pressures could be measured down to 10^{-5} mbar.

These methods rely on the linear relationship between pressure and damping rate. While this linear relationship also holds for translational motion, at low pressures a particle's translational motion is only stable with the addition of feedback cooling [38], which mimics the damping provided by residual gas and therefore complicates the relationship between pressure and damping rate. To first order, the rotational motion is not

affected by feedback cooling [211], making rotational motion a more convenient platform for pressure measurements with levitated particles in lower pressure regimes.

Pressure sensors based on rotating levitated particles offer a number of attractive features, some of which are common to the microviscometers above. In measuring the pressure close to the microparticle surface, they provide a highly-localised probe. This could be extended for high spatial-resolution probing of pressure gradients by using multiple traps or scanning the position of the trap in 3D. Levitated nano- and micro-particles share these features with pressure sensors based on cold atoms [215,216] but can operate at higher pressures than those compatible with atom-trap loading, or indeed with traditional ion gauges. A further possible area of application for optically levitated spinning-rotor gauges is pressure measurements in the presence of magnetic fields, where the magnetically-levitated spinning-rotor gauges are less reliable.

5.4. Temperature sensing and control

As we discussed in Section 4.2, the rotational dynamics of the particle are influenced by the temperature of the surrounding medium in two ways: directly through the thermal-induced Brownian motion, or indirectly through the viscosity of the environment, which for fluids decreases in a non-linear way as the temperature rises. Just as the centre-of-mass translational temperature can be recovered from the width of the position distribution, the temperature can also be inferred from the measured width of the librational mode [83].

In contrast to the librational motion, for an actively rotated particle, the effect of the Brownian fluctuations can be neglected and the rotation rate linked to temperature through the rotational damping rate (see Equation 11). For steady environmental conditions (i.e. constant damping rate), $\omega_{\text{rot}}^{\max}$ linearly increases with the applied laser power (see blue dashed line in Figure 8(a)). Departure from this linear behaviour of $\omega_{\text{rot}}^{\max}$ vs P_{laser} in optically heated rotors has been observed (blue dots and solid line in Figure 8(a)) and used to determine the laser-induced thermal loading [16,147,151,152]. This thermal-to-kinetic energy transfer process has been reported to be able to determine the temperature change with sub-degree accuracy, which is more than one order of magnitude more accurate than measurements done in the same experimental conditions with luminescence-based thermometric techniques that use the thermally induced spectral changes of the particle emission to infer temperature [151]. In addition, the rotational dynamics of the particle can be used to determine the absorption coefficient of the rotating
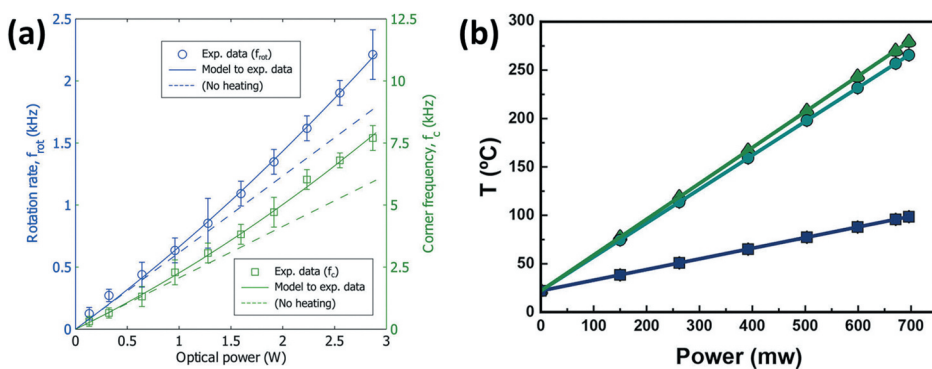
Figure 8. Measurement of temperature using rotation, translation and luminescence. (a) When a particle is heated by laser absorption, the viscosity of the medium decreases. This produces a super-linear increment of the rotation rate as function of the applied laser power (blue circles and solid line), in contrast to theoretical predictions in the absence of heating (blue dashed line) where the rotation rate linearly increases with power. Similar behaviour is observed for the measured vibrational mode (corner frequency) under heating (green squares and solid line) and non-heating (green dashed line) conditions. These deviations from the linear trend can be used to determine the temperatures of the rotational and centre-of-mass modes of the particle, respectively. Adapted with permission from [147]. Copyright 2016 American Chemical Society. (b) Temperatures measured for a birefringent spinning particle as a function of the applied laser power. When the optically trapped spinning particle is not in thermal equilibrium with the environment, the temperature of the internal (green triangles) and the rotational (cyan circles) degrees of freedom differs from that measured for the centre-of-mass (navy squares). Reprinted with permission from [152]. Copyright 2016 American Chemical Society.

particle and the light-to-heat conversion efficiency of non-radiative processes that give rise to the thermal change, even for weakly absorbing particles [147].

The spinning thermometer allows one to measure temperature in a region localised near the particle surface, since the drag torque is generated by the friction of the particle surface with the fluid molecules localised at its surface (see Section 5.2). Thus, a spinning particle can be used as a remote thermometer to measure the extension and magnitude of a thermal gradient with a spatial resolution limited by the particle size [151].

When the particle is in thermal equilibrium with its environment, all degrees of freedom (i.e. internal, translational and rotational) are affected by the same temperature. Thus, the measurement of the internal (from the particle's luminescence), rotational (from ω_{rot}), and centre-of-mass (from ω_q) temperatures of the particle should give a value equal to T_{env} within the experimental error. This is not the case in non-equilibrium thermal conditions when the particle is maintained at a higher or lower temperature than the surrounding medium, as described by the hot and cold Brownian motion theories [217–219], respectively. Perhaps surprisingly, due to the short-range sensing of the spinning degree of freedom, the temperature measured from ω_{rot} equals the internal temperature, and both are higher

than that measured from ω_q [152] (see Figure 8(b)). Therefore, the correction factors needed in the drag coefficient to take into account the temperature change are different for the rotational and translational degrees of freedom [147]. This effect is mainly related to the radial viscosity gradient produced in the vicinity of the particle as the temperature decreases or increases [218], which has been studied for optically heated [147,152,220] and cooled [150,210] particles in liquid.

In vacuum, the temperature of the particle and the environment can be far from equilibrium. Absorption of the trapping laser heats the material, often to temperatures above 1000 K [221,222]. In low-pressure environments, this energy cannot be dissipated by collisions with the background gas but is emitted as blackbody radiation. This results in a recoil force on the particle, which can limit the minimum centre-of-mass temperature and act as a form of decoherence for particles being cooled towards quantum states. Rahman *et al.* showed that the internal temperature of Yb:YLF nanoparticles can be reduced by anti-Stokes laser cooling [83]. Bulk crystals of Yb:YLF have been cooled to sub-cryogenic temperatures [223,224] by careful alignment of the optical field polarisation to the *a*-axis of the crystal; in optically levitated systems the orientational torque ensures this alignment is always achieved [83].

For studies of particles levitated in vacuum, as the pressure around a particle is reduced it is necessary to stabilise the centre-of-mass motion of the particle to avoid particle loss from the trap due to underdamped dynamics [25]. This stabilisation is equivalent to cooling the centre-of-mass temperature. Beyond preventing particle loss, positional stabilisation is advantageous for many applications, such as experiments to measure interactions between a levitated particle and either a nearby surface (see Section 5.5) or a second particle [201,202].

For optically trapped rotors, the centre-of-mass temperature and the variance, or stability, of the rotational mode are inextricably linked, and this can be exploited to manipulate the dynamics of the particle. If a nanorotor explores a large region of the optical trap, the spatial-variation of the light intensity causes a variation in the applied torque, resulting in rotational modes with larger variance. Therefore, by applying feedback cooling to damp the translational motion of rotors, the stability of the rotational mode can be improved [225]. This can be considered to be a form of cooling of the rotational motion.

In complementary observations, gyroscopic stabilisation of the translational motion [145,213] and the orientation [173] has been observed by rotating particles at high speed. Coupling of rotational and translational degrees of freedom has also been shown for certain lower-symmetry particle morphologies, such as disks [226], while coupling between rotational and

translational modes can also be enhanced in an optical cavity [227,228] or by painting a spot on the surface of a sphere and performing a continuous joint measurement of two motional modes [229]. For dumbbell-shaped particles, where the moments of inertia of the various rotational modes are comparable, the spinning motion about the symmetry axis couples the two degrees of librational motion, which results in precessional motion [167,230].

Narrow oscillator linewidths (i.e. more stable motion) offer advantages in force and torque sensing (see Section 5.5). To observe Casimir torques with particles close to large surfaces, stabilisation of the translational motion will only serve to fix the separation. To observe these effects with a fixed orientation, the librational motion will also need to be cooled [231]. Proposals to measure gravitational waves with levitated disks also requires cooling of the orientational degree of freedom [232]. For spinning motion, van der Laan *et al.* showed that feedback cooling of the translational motion narrowed the linewidth of the rotational motion [225], while Kuhn *et al.* have achieved µHz-level linewidths by driving the spinning motion with a periodically modulated polarisation [213]. Bang *et al.* [233] recently reported cooling of all translational modes plus both librational modes of optically-levitated nanodumbbells, reaching temperatures below 5 K for the translation and around 10 K for the librational modes. The remaining degree of freedom, about the long axis of the dumbbell, was free to undergo rotation and perturbs the librational modes. Pan *et al.* propose harnessing the rotational Doppler effect, in analogy with laser cooling of neutral atoms, as an alternative method to cool the rotational motion [234].

Motivated partly by cooling the motion of the levitated particle, an area of active research in levitated optomechanics is the coupling of levitated oscillators to other quantum systems such as ultracold atoms [118,235,236]. An alternative coupling can be generated for levitated nano-diamonds: coupling of the translational [237] or librational [238–240] state of the particle to the spin-states of embedded nitrogen-vacancies. Recently, Delord *et al.* showed manipulation of the librational motion of a levitated 15 µm-diamond by microwave-control of the spin-state of nitrogen-vacancies within the diamond [241]. The approach is reminiscent of observations in trapped ions and neutral atoms, where the coupling of the electronic state of the atom to its external motion is regularly harnessed to cool the motion of the particle [242,243] or for the creation of controlled quantum dynamics [244]. In particular, Delord *et al.* observed a spin-state dependent torque on the particle. By red-detuned microwave-manipulation of the spin-states of the nitrogen vacancies, the librational motion of the diamond was cooled from room temperature to 80 K. Ground-state cooling of the librational mode promises to be attainable for a hybrid particle

comprising a higher-purity, smaller, diamond crystal attached to a ferromagnet [245].

5.5. Force and torque sensing

High-resolution force and linear motion detection has been realised with optical tweezers in liquid medium [7]. In some cases, this is not sufficient to completely characterise the dynamics of biological processes or the mechanics of intracellular entities. For example, DNA forms a double strand of twisted single-DNA fibres that undergoes different dynamics depending on the applied tension and torsional stress. Optical trapping in combination with a microaspiration pipette technique was used to study the rotational dynamics of a double DNA strand subjected to different tensional forces applied by beads attached to opposite ends of the molecule [246]. The authors showed that an over- or underwound DNA molecule behaves as a wind-up motor, storing energy and releasing it at a constant torque. Additionally, they demonstrated that an overstretched molecule can be used as a force–torque converter. In this technique, the applied torque is produced by the rotation of the micropipette that holds one end of the molecule of DNA, and the rotation of the molecule is detected by a probe particle attached to its central part.

Since the 18th Century, some of the most sensitive detections of forces have been accomplished through measurements of rotation by using a torsion balance (Figure 9(a)). Examples include Coulomb in his pioneering work measuring electrostatic forces [247], Cavendish establishing the gravitational constant [248], Lebedew measuring radiation pressure forces [249] and Beth measuring the angular momentum of light [88].

A torsion balance can be realised by attaching a DNA strand to an asymmetric particle, i.e. a non-spherical [250] or birefringent [140,251,252] particle, able to orient in linearly polarised light due to the orientation torque (see Section 3.1.1). When the polarisation plane is rotated, the particle reorients and the attached DNA molecule is twisted and torsionally stressed. The torsional strain of the molecule acts against the applied optical torque and can be measured from the angular displacement between the laser polarisation and the particle. This method allowed Oroszi *et al.* [250] to directly control and measure the magnitude of the applied optical torque on a 2μm-diameter polystyrene disk and characterise the torsional modulus of the DNA molecule with a precision comparable to that reported by [246].

An optical microprotractor and torsion balance can also be constructed with an optically trapped birefringent liquid crystal particle (Figure 9(d,e)) to fully characterise the dynamics of individual Kinesin motors, including the rotation and torque generated by the molecule when it walks along a microtubule transporting a cargo [47]. These motors use the free energy
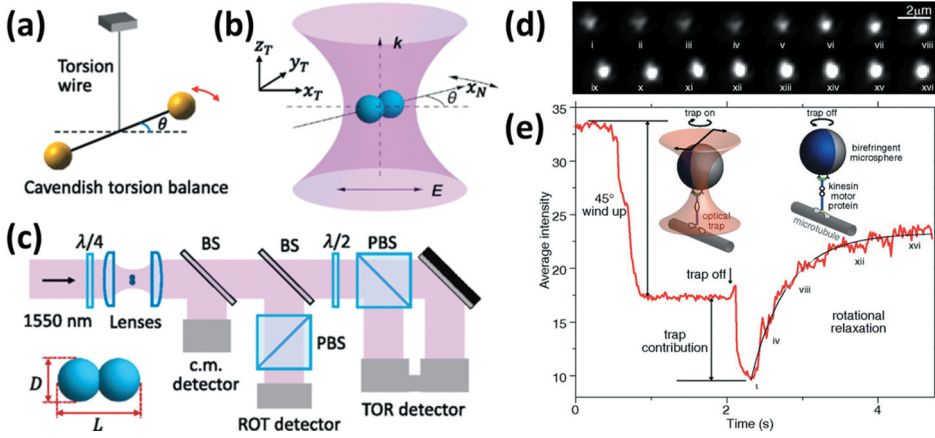
Figure 9. Optically trapped torsion balance. (a) The original Cavendish torsion balance detected forces when the lead spheres twist the wire. (b) When external forces change the orientation of the trapped particle in a linearly polarised optical tweezers, the polarisation of the optical tweezers can be used as a probe of the force. (c) Simplified setup for the control and detection of rotational motion. Reprinted figure with permission from [81]. Copyright (2018) by the American Physical Society. (d-e) The optical torque exerted by a Kinesin molecular motor can be measured using a birefringent liquid crystal particle attached to the molecule. The rotation is detected by cross-polarisation microscopy (d), resulting in a change of intensity in the image of the particle (e). An initial torsional stress is applied by optical torque on the birefringent particle ('wind up' phase – left inset). The torsional stiffness of the molecular motor can be extracted from the rotational relaxation time after the optical torque is switched off ('rotational relaxation' phase – right inset). Reprinted with permission from [47].

available ($\sim$100 pN nm) from the hydrolysis of ATP molecules to exert work. Using the fact that, in the torsion balance, the motor torque is equal to the optical torque, Ramaiya *et al.* measured the torque produced by the molecule to be 170 $\pm$ 20 nm/rad, and a torsional stiffness of 54 $\pm$ 7 nm/rad. These values, together with the characterisation of the translational motion, allowed them to measure the total work per step performed by the motor as 77 $\pm$ 16 pN nm. This proved that Kinesin is a highly efficient molecular motor with an efficiency of $\sim$80%.

The force sensitivity $S_F^{1/2}$ of an oscillator coupled to an external bath at temperature T_{env} is given by the thermal-noise force spectral density.

$$ S_F^{1/2} = \sqrt{\frac{4\kappa_{\mathrm{q}} k_{\mathrm{B}} T_{\mathrm{env}}}{\omega_{\mathrm{q}} Q_{\mathrm{q}}}}. \tag{14} $$

and averaging over long integration times b^{-1} allows the detection of forces as small as $F_{\mathrm{min}} = S_F^{1/2} b^{1/2}$. Given the potential long integration times, high oscillation frequencies and mechanical quality factors, nano- and micro-scale oscillators in vacuum are attractive for force sensing. Cryogenically cooled tethered oscillators can achieve force sensitivities below 12 zN Hz$^{-1/2}$ [253].

Much of the motivation for performing force-sensing experiments with levitated particles, compared to their tethered counterparts, comes from the potential to significantly increase Q by decreasing the coupling to the thermal environment. In the case of levitated particles without feedback cooling,[11]

$$F_{\min} = \sqrt{4k_{\mathrm{B}}T_{\mathrm{env}}M\Gamma_q b}. \tag{15}$$

Force sensitivities on the order of 10^{-20} N Hz$^{-1/2}$ have been demonstrated for the translational motion of particles [254,255], allowing the measurement of 30 zN electrostatic forces within 10s. After 10^5 s of integration, Ranjit et al. were able to obtain a minimum measurable force of ∼6 zN [24] for a 300 nm silica nanosphere. This sensitivity opens up a variety of force-sensing applications, such as the measurement of electric fields [24,255], short-range forces [28], high-frequency gravitational waves [232], quantum collapse models [32], and tests of the inverse-square law of gravity on short length scales [25].

Rotational motion can further enhance the measurement of forces. Experiments tracking the translational motion of levitated microspheres in large electric fields set an upper bound for the probability of the existence of milli-charges $> 10^{-5}e$, which were proposed to partially explain the existence of dark matter [256]. Using translational motion of a neutrally charged optically trapped microsphere in vacuum, Rider et al. [257] searched for screened interactions associated with dark energy by bringing the microsphere to within 20 μm of an oscillating cantilever. Their results placed an upper-bound on the strength of such interactions to 0.1 fN. In both experiments, it was proposed that the sensitivity limits could be lowered further by spinning the particles to average out the contributions of fixed electric dipole moments in the particles.

Complementary to measurements with translation, tracking the rotational motion of particles levitated in vacuum also offers a route to precision sensing. The vast majority of force sensing with trapped particles requires the force to vary at or near the trapped particle's resonant frequency, where the mechanical response of the particle is largest. By frequency-locking the rotation of a silicon nanorod to an external clock via pulses of circularly polarised light and measuring the phase-lag between the optical drive and the response of the nanorod, Kuhn et al. demonstrated an alternative force-sensing scheme [213]. As the phase lag changes under application of an external force, and with freedom to choose the clock frequency, the method can probe forces with a torque sensitivity of 10^{-22} N m Hz$^{-1/2}$ without being tied to the oscillator's resonant frequencies.

Similarly to Equation 14, the minimum detectable torque $\tau_{\min}$ for a rotor coupled to a thermal bath at temperature T_{env} is

$$\tau_{\min} = \sqrt{\frac{4k_B T_{\text{env}} I \omega_\theta b}{Q_\theta}}. \tag{16}$$

The original Cavendish experiment measured a torque of about 10^{-7} N m caused by gravitational attraction. Modern cavity-optomechanical torque sensors have a torque sensitivity as low as 3×10^{-24} N m Hz$^{-1/2}$ [258] after cryogenic cooling and can be used to probe small-scale magnetism [259] and Casimir forces [260]. Recently, a 10 mg-mass torsion pendulum was demonstrated with 20 aN m Hz$^{-1/2}$ sensitivity. In the case of optically levitated torque sensors, the analogue to Equation 15 is

$$\tau_{min} = \sqrt{4k_B T_{\text{env}} I \Gamma_{\text{rot}} b}. \tag{17}$$

Optically levitated torque sensors have been demonstrated using nanodiamond ellipsoids [75], silicon nanorods [213], silica clusters [167] and silica nanodumbbells [49], with torque sensitivities below 10^{-22} N m Hz$^{-1/2}$. A typical system is illustrated in Figure 9(c). Most recently, Ahn *et al*. demonstrated an optically levitated and spinning nanodumbbell, held in vacuum at room temperature, achieving a torque sensitivity as low as 4×10^{-27} N m Hz$^{-1/2}$ [49]. This surpasses the sensitivity of state-of-the-art cryogenically cooled tethered oscillators by three orders of magnitude.

The sensitivity of these schemes is currently limited by the frequency-stability of the rotational motion, which in turn is limited by coupling to thermal fluctuations of the environment [225]. The frequency stability can be improved by driving the rotational motion [213] or by feedback cooling of the transverse motion [225] to ensure constant torque application, resulting in $Q_\theta \sim 10^{12}$ [213]. Proposals for six-dimensional cooling of the translation and rotational modes into the quantum regime suggest attainable torque sensitivities of 10^{-30} N m Hz$^{-1/2}$ [261].

A different, as yet unrealised, avenue to sensitive rotation detection was proposed by Shi & Bhattacharya [227]. Confining a dielectric sphere in an optical cavity which is pumped with a Laguerre-Gaussian mode will induce orbital motion of the particle. Pumping the cavity with multiple Laguerre-Gaussian modes makes a sensitive rotation detector.

Among the most-anticipated applications for levitated rotating particles are tests of quantum and vacuum friction. Quantum electrodynamics predicts that virtual particles are constantly created and annihilated, and that the vacuum electromagnetic field is therefore constantly fluctuating. These fluctuations lead to phenomena such as the Casimir effect [262], but the debated [263,264] quantum and vacuum friction still remain unobserved in experiments. These phenomena may soon be investigated using optically levitated rotating particles, due to the impressive torque sensitivities and rotation rates already demonstrated.

Vacuum friction is the drag force exerted on a surface as it moves through a vacuum. Due to quantum fluctuations, the vacuum electromagnetic field acts as a complex fluid. As an object moves through this field, its energy is dissipated by the ejection of photons and the motion is damped [265]. Manjavacas *et al.* considered the vacuum friction acting on isolated rotating particles [51,52]. They predicted that vacuum friction should give rise to a stopping time on the order of days for a 10 nm graphite particle with a rotational frequency on the order of 10s of GHz. Such a weak frictional force requires a particle spinning in place, rather than undergoing translational motion, in order for these dynamics to be visible. Although this particle size and rotation rate are outside the ranges demonstrated in experiments so far, measurements of single nanoparticles in optical potentials are now routinely performed over many days [24,25,213].

Quantum friction was first proposed by Pendry [266], who considered two dielectric surfaces, separated by a finite distance in vacuum, moving parallel to each other at constant speed. Zero-point charge fluctuations on the surfaces interact with each other to generate a friction which opposes the motion. Zhao *et al.* extended the scenario to consider a nanosphere rotating near a surface [53]. They found that the frictional force should be several orders of magnitude larger than for the same sphere rotating in vacuum. The quantum friction should be largest for semiconductor materials due to the excitation of surface plasmon polaritons. Ahn *et al.* calculated the magnitude of the quantum frictional torque exerted on a 150 nm diameter silica nanosphere rotating at 1 GHz within 200 nm of a silica surface (chosen to match the phonon polariton modes of the particle). They found that for a temperature of 350 K the quantum frictional torque is $> 10^{-28}$ N m [49]. Importantly, this is larger than the air damping torque at 10^{-9} mbar, a pressure within reach of those at which optical levitation of nanoparticles has already been achieved [43]. This certainly suggests that tests of quantum friction may be possible in the near future: levitated nanospheres have now been trapped at sub-wavelength distances from surfaces [267], and stabilisation of the relative position of particle and surface may be accomplished using either gyroscopic stabilisation [145] or feedback cooling of the translational motion [37,38,233]. Similarly, Xu and Li calculated that measurements of the torque exerted due to Casimir effects between a librating, levitated nanorod and a flat birefringent plate [231] are also within reach of state-of-the-art experiments. Further proposals suggest that the Casimir torque may be harnessed to produce lateral forces on the rotating particle [268,269] and for non-contact transfer of angular momentum between nanoparticles [270,271].

5.6. Rotational tests of the quantum-classical interface for massive objects

An important open topic in modern physics is the extent to which quantum physics holds in the classical world, and much research is currently devoted to testing the quantum superposition principle (where an object appears to be in multiple different states at the same time) with increasingly macroscopic systems [272–274], including ultracold atomic gases [275,276], large molecules [277,278] and tethered mechanical oscillators such as membranes and cantilevers [279,280]. Part of the motivation for these studies is for technological impact. The already-impressive sensing performance of classical levitated particles offers promise of even further sensitivity in the quantum regime [281]. There is currently rapidly-increasing interest in the development of quantum sensors to provide commercial quantum technologies [282,283].

The most massive of the candidates in these tests are the optomechanical systems where the flexural oscillation of a cantilever or membrane is monitored and controlled via coupling to an optical cavity electromagnetic field. This coupling has been harnessed to cool such oscillators to the ground state [284,285], and these systems show remarkable promise for quantum technologies and force sensing [286]. However, there are some key advantages that a *levitated* oscillator offers over such a tethered system.

The low coupling to the environment of levitated particles avoids one of the principal limitations of tethered state-of-the-art optomechanical systems. In the context of quantum optomechanics, coupling between the optomechanical device and the environment leads to decoherence of the quantum state, which can be reduced by cooling to cryogenic temperatures but still provides a restriction to the fidelity of quantum protocols. The removal of a tether to the environment is one of the principal motivators for optical levitation experiments, which therefore are able to operate in room temperature environments, and mechanical quality factors as high as 10^{12} have been proposed [27]. Levitated systems also offer other potential advantages over their tethered counterparts. Examples include the ability to control the coupling to the environment (offering the opportunity for investigations of nanoscale thermodynamics [196,287]); the ability to be released from the potential and be recaptured [288]; the potential to realise macroscopically separated quantum superposition states [273]; but also the ability to investigate rotational degrees of freedom,[12] which will be our main focus here.

Given the impressive control, measurement sensitivity, and recent success in cooling to the ground state (see Section 5.4 and Section 5.5), optically trapped particles held in vacuum offer an exciting test bed for fundamental physics. A particular motivation for levitated systems is to create positional superpositions over length-scales larger than the constituent particles

themselves. The generation of macroscopic quantum superposition states is predicted [26], and promises to provide insight into wavefunction collapse models [29,31], to shed light on quantum gravity [36] and dark matter [33], and to open up avenues in quantum sensing [28]. For a recent review of progress in tests of quantum physics with levitated particles, see [22].

While cooling of nanoparticles to the translational ground state has been recently achieved [44], this has not yet been replicated for the rotational degrees of freedom. A variety of proposals exist for cooling trapped particles to the rotational ground state, which go beyond the cooling techniques covered in Section 5.4.

Librational modes of oscillation make good candidates for quantum levitated optomechanics experiments, as the librational modes oscillate at higher natural frequencies than the translational modes (see Section 3.1.1) and thus the rotational ground state energy is raised. Hoang *et al.* showed that the librational modes exist at higher frequencies than the translational ones for the same experimental parameters, and theoretically proposed using an auxiliary linearly polarised cavity field to drive cavity cooling of the librational mode of a non-spherical nanoparticle held in a separate optical tweezer [75]. Compared to the translational mode, cavity cooling to the ground state was found to be feasible under a wider range of cavity field strengths and cavity lengths. Proposals have also been made for reaching the ground state of librational motion via active feedback cooling for ellipsoidal particles [84], while Seberson *et al.* showed that an asymmetric potential generated by elliptical polarisation or by using two perpendicular laser beams may also allow ground-state cooling of the libration [230]. This latter scheme has very recently been implemented by Bang *et al.* [233], although the librational temperatures they achieved remain in the Kelvin regime. High-purity nanodiamond/ferromagnet hybrid particles have also been proposed as a promising candidate for librational ground-state cooling [245].

Although the high librational frequencies make the torsional modes appealing candidates for ground-state cooling, decoherence caused by shot noise due to photon scattering could actually make it more challenging to cool the librational modes than the translational modes [289]. The question of whether the decoherence rate is stronger for translation or libration was studied in [289], where it was found that the relative heating of rotational and translational motion depends on the size and morphology of the particle and the properties of the trapping beam. It was suggested that rotational heating is lower for nanoellipsoids with lower ellipticity. Schäfer *et al.* have also shown that the librational modes are weakly affected by photon scattering, improving coherence times by around one order of magnitude when compared to other motional modes [261] and making the librational mode appealing for future experiments in rotational quantum optomechanics.

Even more appealing than cooling a particle to its librational ground state is the prospect of simultaneous cooling of all motional degrees of freedom to the ground state. While the ro-vibrational ground-state has been obtained for diatomic molecules [290], the ro-translational ground-state of levitated particles has not yet been obtained. However, the wide variety of experimental platforms already studying rotational levitodynamics suggest that this will be extended to rotational degrees of freedom in the near future. Stickler *et al.* [74] proposed cavity cooling to the ground state for rods and disks by exploiting alignment-dependent coupling between an asymmetric particle and a cavity field, which was first seen experimentally in [55]. Schäfer *et al.* have proposed a method to allow full six-dimensional cooling of the motion of non-spherical nanoparticles to the ground state, by coherent scattering of elliptically shaped and polarised trapping light into a transverse optical cavity [261].

The physics of libration and spin offer interesting differences in the quantum realm [227]. As libration is an example of a harmonic oscillator, it is a linear system with evenly separated energy eigenvalues with a finite ground state energy. In many cases, a nonlinear interaction (such as may be provided by coupling to a cavity) is required to observe the differences between a classical and a quantum oscillator. The spinning rotor is an inherently nonlinear system with an anharmonic energy spectrum and a ground state energy of zero, i.e. the particle ceases its rotational motion entirely.

Early work to create superposition states using rotational degrees of freedom proposed the use of multiple Laguerre-Gaussian modes in a cavity to cool the librational mode of a nanorod [26], microwindmill [291] or even a rod-shaped virus [26] to the ground state, although this scheme has not yet been demonstrated experimentally.

While many of the schemes to observe positional superpositions of the centre-of-mass mode require low translational temperatures, experiments with rotation may circumvent this requirement. Stickler *et al.* have proposed a method which could probe the quantum-classical interface by observing quantisation of the rotational degree-of-freedom of optically levitated nanorods [292], which does not require cooling to the ground-state. In their proposal, which is illustrated in Figure 10(a), a nanorod (with the rotational motion cooled to below 1 K) is optically levitated inside a vertically oriented optical cavity, and set into a well-defined initial orientation angle given by the polarisation angle of the cavity light field. The nanorod is released from the trap and its orientation state disperses into a superposition of all angles [293,294]; a coherent evolution back to its original orientation should be observable at integer multiples of a characteristic quantum revival time [295], due to fully constructive interference of all the rotation states. As well as investigating the role of quantum mechanics at mesoscopic length-scales,
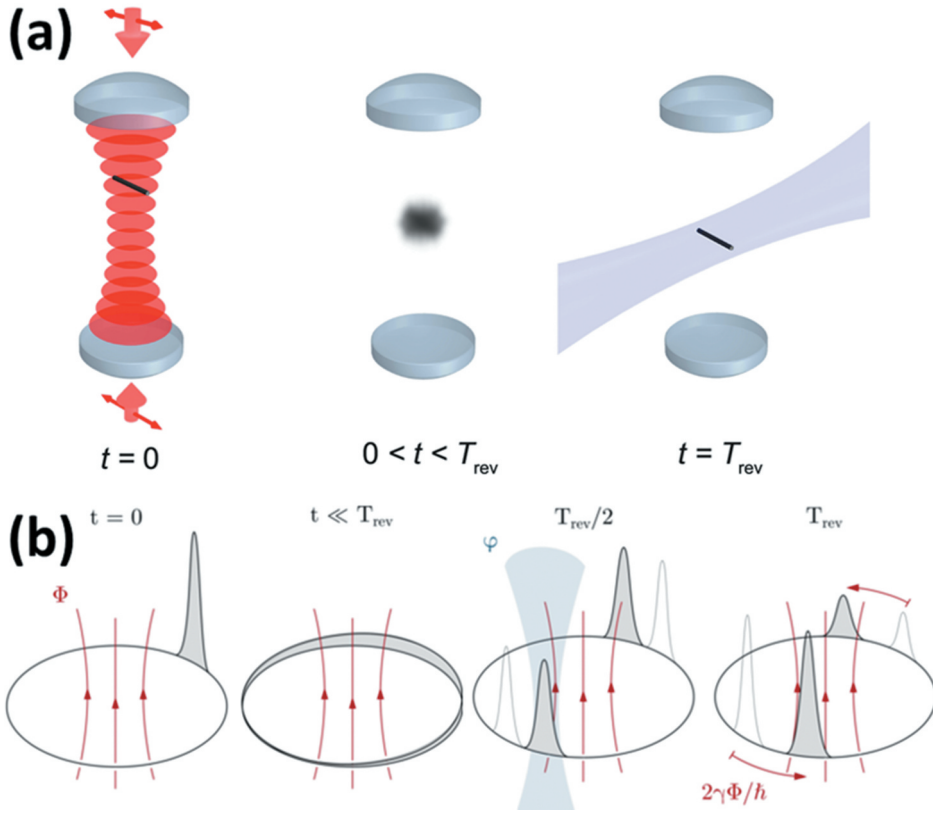
Figure 10. Rotational quantum superposition. Quantum revivals of (a) spinning [292] (CC BY 3.0) and (b) orbiting nanoparticles [304] (CC BY 4.0) are a signature of macroscopic superpositions of the rotational states.

the approach offers promise as a quantum sensor of external torques: the orientational revival signal will be sensitive to both the magnitude and direction of any external torque, detecting torques on the order of 10^{-30} N m, which is orders of magnitude beyond existing experiments with levitated particles [49]. A quantum torsion balance realised by placing a nanorod in a librational superposition state has been proposed for testing the quantum nature of gravity [296].

The orientational revival approach has also been suggested as a test of one of the most prominent quantum collapse models (Continuous Spontaneous Localisation, or CSL). Such collapse models are modifications of the Schrödinger equation which attempt to provide an explanation both for the apparent lack of superposition phenomena on macroscopic scales, and of the measurement-induced collapse of quantum mechanical wavefunctions. The effects of CSL should cause an increased spread across orientation angles of the nanorod's wavefunction [297]. The rotational degrees of freedom of a levitated disk have been shown to offer an increased sensitivity to

CSL-induced decoherence when compared to translational motion [298,299], while Carlesso *et al.* [300] offer an alternative, non-interferometric test of CSL using the rotational modes of a trapped rod coupled to an optical cavity.

It will be important to distinguish decoherence due to wavefunction collapse from more mundane sources such as background gas or Rayleigh scattering of photons, which have been studied in [289,301]. The rotational degrees of freedom have been suggested to be less influenced by decoherence than the translational states [302]. By tailoring the shape of the trapped particle, the rotational motion can be made robust against decoherence sources without significant reduction of the sensitivity for quantum sensing [303].

Complementary to superpositions of the orientation of a particle, Kialka *et al.* [304] propose a scheme for realising matter-wave interference which could be realised with *orbiting* levitated nanorotors, also based on quantum revivals (Figure 10(b)). In a ring trap, an initially localised quantum state disperses along the circumference at a rate determined by the angular momentum uncertainty (which can be reduced using the aforementioned cooling techniques). At a later time, due to quantisation of the orbital angular momentum, the spreading is reversed and the state relocalises. The method can be used as a sensor of external fields, which cause imperfect reformation of the initial state, in a system reminiscent of cold atom sensors based on matter-wave guiding around ring traps [305–307].

Moving beyond the generation of superposition states, there are also proposals to entangle the rotational modes of particles with the translational state. Entanglement between the translational coordinates and the orientation degrees of freedom of an asymmetric rotor can be generated by a single-slit interference experiment [308], when the de Broglie wavelength of the particle is comparable to or larger than both the width of the slit and the classical extent of the particle. An alternative proposal to engineer entanglement between translational and rotational modes proposes continuous measurement of a point on the surface of the sphere [229], a route not available when working with atomic or molecular systems. Finally, Xiao *et al.* have proposed protocols to generate squeezed states of the librational mode of a levitated particle by driving the oscillation [309].

Another possibility to observe superposition states without low translational temperatures is presented by experiments with nitrogen-vacancy (NV) centres in nanodiamond. In analogy with trapped atomic ions, which have a rich history of use as spin-mechanical systems where the internal state of the atoms is coupled to their external motion [244], the state of the electron spin of the NV-centre can be coupled to (and therefore interrogated by) the classical rotation [310]. This can even be used to control and cool the classical motion of the nanodiamond [241]. While similar

coupling can be achieved between the NV spin-state and translational motion [237,311], using the rotational degree of freedom offers a technical advantage in that strong coupling between the spin-state and the external degrees of freedom is realised without the need to use very strong magnetic field gradients [238,239]. This opens up the prospect of investigating many-body quantum phase transitions and Schrödinger cat states where the rotation of the nanodiamond and the spin-state of a single NV-centre are entangled [239]. Many proposals for experiments with the translational modes also benefit from orientational stabilisation (librational cooling) to stabilise the alignment of the NV-centre [75].

While red-detuned microwave-manipulation of the spin-states of the NV centres in levitated diamond particles can potentially cool the librational motion to the ground state [241] (see also Section 5.4), blue-detuned microwave manipulation increases the energy of the libration and generates self-sustained, laser-like oscillations in the rotational equivalent of the optical-tweezer phonon laser [312]. Rapidly rotating NV-centres have been suggested as a platform for enhanced quantum sensing [313]. Driving the motion through spin-motional coupling opens the potential to generate non-classical states of motion of the particle by appropriate spin-manipulation, and for quantum non-demolition measurements of the spin-state by tracking the external motion.[13]

6. Conclusions

In this article we have reviewed the physical origins and applications of rotational motion in optical traps. We discussed how the optical torque may be tailored by designing the material properties of the particle and controlling the characteristics of the light field, and how the maximum achievable rotational speed is limited by the environment. The librational, spin and orbital degrees of freedom offer significant differences to the more traditionally considered translational motion, and these differences have already been harnessed in liquid environments as micropumps, sensors of viscosity and temperature, and offered key insights into the nature of the orbital angular momentum of light.

In the underdamped regime, exciting new directions are emerging. Particles can be made to spin at GHz rates, opening a window to explore the material properties of trapped objects under extreme conditions. Sublime torque and force sensitivities have been demonstrated, which promise to soon answer open questions in fundamental physics: testing the origins of dark matter and dark energy, the existence of vacuum and quantum friction, and probing the boundary between classical and quantum physics. What is clear is that spinning particles in optical traps will continue to usher in new revolutions in science.

Notes

1. The forces on particles much larger than the wavelength of the trapping light (the Mie regime) can be intuitively understood by considering a ray optics picture. In the Rayleigh regime, where the particle is much smaller than the wavelength, it is necessary to consider the particles as individual electric dipoles that interact with the field and are high or low field seeking. In the intermediate regime the generalised Lorenz-Mie scattering theory can be applied to model the forces. A detailed discussion of the calculation of optical forces can be found in [1,314].

2. Optical forces are not the only mechanism for introducing rotational motion to trapped particles. For example, electrostatic traps can couple to the fixed electric dipole moment of particles [214,315], and application of time-varying voltages used to spin the particles. Alternatively, in air and liquid, acoustic forces can be used to manipulate the particles [316].

3. The separation of the angular momentum into its spin and orbital parts is a matter of debate and their origin is still controversial [177,317]. Here, we will focus on the rotational motions produced by the interaction of the trapped particle with the angular momentum, without analysing the existence or origin of its components.

4. Highly-absorbing particles, unlike dielectric particles, cannot be trapped in the high intensity region of the beam unless additional confinement along the axial direction is provided, as the scattering force overcomes the gradient force. For example, this axial confinement was generated in [104] by using a trapping beam blue-detuned from the plasmon resonance of metallic particles, which creates a repulsive optical force that pushes the particles against the top coverslip of the microfluidic chamber. Particles smaller than the Laguerre-Gaussian ring diameter are confined within the dark region at the centre of the beam, where scattering still produces an orbital rotation about the beam axis [104].

5. Most commonly in optical trapping, static [98,102,318] or computer-generated [105,319] phase masks are used to convert fundamental Gaussian modes into beams of arbitrary amplitude and phase. This allows the engineering of beam profiles with independent control over the trapping geometry (dictated by the amplitude) and the transverse momentum (governed by the phase gradient). An example of this flexibility is the so-called 'perfect' vortex beams, where the diameter of the bright intensity ring is independent of ℓ, lifting the coupling of trapping geometry and angular momentum that is given by the Laguerre-Gaussian beams [320,321]. This therefore allows high values of ℓ to be transferred to particles without the limitation of large beam radius that is present for Laguerre-Gaussian beams. Tailoring the phase and amplitude of light even further allows one to go beyond simple circular orbits and to engineer motion around more complicated paths, e.g. [130,322–325].

6. In plasmonic devices heating of the substrate and subsequently the environment is of particular concern, as the thermophoretic and convective forces can overcome the optical forces [326,327], although these may be mitigated by using plasmonic nanotweezers with integrated thermal management [56].

7. Note the discrepancy with [135].

8. Interestingly, the partial reflection of linearly polarised light by these chiral polymeric liquid crystal particles can produce an optical torque able to set the particle into rotation, as observed by Hernández *et al.* [170]. Intriguingly, they saw on-axis trapping and spinning for small ($a < 5\mu m$) particles, but off-axis trapping and orbiting for larger particles.

9. The dependence of rotation rate on mass, volume and shape of a rotor which had been surface-functionalised with an appropriate biomolecule was recently shown to be sufficiently sensitive to detect the presence of single cells or bacteria [328].

10. See footnote 5.

11. In the case of a feedback-cooled particle, the product $\Gamma_q T_{env}$ can be substituted for $\Gamma_{eff} T_{eff}$, where Γ_{eff} is the effective damping due to the feedback and T_{eff} is the resultant effective temperature.

12. We note that libration or torsional motion [258] and orbital motion [329] have been demonstrated with tethered oscillators, but free spinning of such systems is not possible.

13. An alternative quantum non-demolition measurement of rotation has been proposed for levitated He droplets in [330].

Disclosure statement

The authors declare no conflict of interest.

Funding

ORCID

Graham D. Bruce ⓘ http://orcid.org/0000-0003-3403-0614
Paloma Rodríguez-Sevilla ⓘ http://orcid.org/0000-0003-4743-6576
Kishan Dholakia ⓘ http://orcid.org/0000-0001-6534-9009

References

[1] Jones PH, Maragò OM, Volpe G. Optical tweezers: principles and applications. Cambridge University Press (Cambridge, UK); 2015.

[2] Barredo D, Lienhard V, De Leseleuc S, et al. Synthetic three-dimensional atomic structures assembled atom by atom. Nature. 2018;561:79–82.

[3] Kimura Y, Bianco PR. Single molecule studies of DNA binding proteins using optical tweezers. Analyst. 2006;131:868–874.

[4] Ashkin A, Dziedzic JM. Optical trapping and manipulation of viruses and bacteria. Science. 1987;235:1517–1520.

[5] Thalhammer G, Steiger R, Bernet S, et al. Optical macro-tweezers: trapping of highly motile micro-organisms. J Opt. 2011;13:044024.

[6] Svoboda K, Block SM. Biological applications of optical forces. Annual Review of Biophysics and Biomolecular Structure. 1994;23:247–285.

[7] Capitanio M, Pavone F. Interrogating biology with force: single molecule high-resolution measurements with optical tweezers. Biophys J. 2013;105:1293–1303.

[8] Rodríguez-Sevilla P, Labrador-Páez L, Jaque D, et al. Optical trapping for biosensing: materials and applications. J Mater Chem B. 2017;5:9085–9101.

[9] Favre-Bulle IA, Stilgoe AB, Scott EK, et al. Optical trapping in vivo: theory, practice, and applications. Nanophotonics. 2019;8:1023.

[10] Block SM, Goldstein LSB, Schnapp BJ. Bead movement by single kinesin molecules studied with optical tweezers. Nature. 1990;348:348–352.

[11] Svoboda K, Schmidt CF, Schnapp BJ, et al. Direct observation of kinesin stepping by optical trapping interferometry. Nature. 1993;365:721–727.

[12] Bugiel M, Fantana H, Bormuth V, et al. Versatile microsphere attachment of GFP-labeled motors and other tagged proteins with preserved functionality. J Biol Methods. 2015;2:30.

[13] Ashkin A, Dziedzic JM. Internal cell manipulation using infrared laser traps. Proc Natl Acad Sci USA. 1989;86:7914–7918.

[14] Johansen PL, Fenaroli F, Evensen L, et al. Optical micromanipulation of nanoparticles and cells inside living zebrafish. Nat Commun. 2016;7:10974.

[15] Favre-Bulle IA, Stilgoe AB, Rubinsztein-Dunlop H, et al. Optical trapping of otoliths drives vestibular behaviours in larval zebrafish. Nat Commun. 2017;8:630.

[16] Parkin SJ, Knöner G, Nieminen TA, et al. Picoliter viscometry using optically rotated particles. Phys Rev E. 2007;76:041507.

[17] Rodríguez-Sevilla P, Zhang Y, de Sousa N, et al. Optical torques on upconverting particles for intracellular microrheometry. Nano Lett. 2016;16:8005–8014.

[18] Rodríguez-Sevilla P, Sanz-Rodríguez F, Peláez RP, et al. Upconverting nanorockers for intracellular viscosity measurements during chemotherapy. Adv Biosyst. 2019;3:1900082.

[19] Martínez IA, Roldán, É, Dinis L, et al. Brownian Carnot engine. Nat Phys. 2016;12:67–70.

[20] McCann LI, Dykman M, Golding B. Thermally activated transitions in a bistable three-dimensional optical trap. Nature. 1999;402:785–787.

[21] Ashkin A, Dziedzic J. Feedback stabilization of optically levitated particles. Appl Phys Lett. 1977;30:202–204.

[22] Millen J, Monteiro TS, Pettit R, et al. Optomechanics with levitated particles. Rep Prog Phys. 2020;83:026401.

[23] Li T, Kheifets S, Medellin D, et al. Measurement of the instantaneous velocity of a Brownian particle. Science. 2010;328:1673–1675.

[24] Ranjit G, Cunningham M, Casey K, et al. Zeptonewton force sensing with nanospheres in an optical lattice. Phys Rev A. 2016;93:053801.

[25] Monteiro F, Li W, Afek G, et al. Force and acceleration sensing with optically levitated nanogram masses at microkelvin temperatures. Phys Rev A. 2020;101:053835.

[26] Romero-Isart O, Juan ML, Quidant R, et al. Toward quantum superposition of living organisms. New J Phys. 2010;12:033015.

[27] Chang DE, Regal CA, Papp SB, et al. Cavity opto-mechanics using an optically levitated nanosphere. Proc Natl Acad Sci USA. 2010;107:1005–1010.

[28] Geraci AA, Papp SB, Kitching J. Short-range force detection using optically cooled levitated microspheres. Phys Rev Lett. 2010;105:101101.

[29] Romero-Isart O. Quantum superposition of massive objects and collapse models. Phys Rev A. 2011;84:052121.

[30] Romero-Isart O, Pflanzer AC, Blaser F, et al. Large quantum superpositions and interference of massive nanometer-sized objects. Phys Rev Lett. 2011;107:020405.

[31] Bassi A, Lochan K, Satin S, et al. Models of wave-function collapse, underlying theories, and experimental tests. Rev Mod Phys. 2013;85:471–527.

[32] Bateman J, Nimmrichter S, Hornberger K, et al. Near-field interferometry of a free-falling nanoparticle from a point-like source. Nat Commun. 2014;5:4788.

[33] Bateman J, McHardy I, Merle A, et al. On the existence of low-mass dark matter and its direct detection. Sci Rep. 2015;5:8058.

[34] Wan C, Scala M, Morley GW, et al. Free nano-object Ramsey interferometry for large quantum superpositions. Phys Rev Lett. 2016;117:143003.

[35] Romero-Isart O. Coherent inflation for large quantum superpositions of levitated microspheres. New J Phys. 2017;19:123029.

[36] Bose S, Mazumdar A, Morley GW, et al. Spin entanglement witness for quantum gravity. Phys Rev Lett. 2017;119:240401.

[37] Li T, Kheifets S, Raizen MG. Millikelvin cooling of an optically trapped microsphere in vacuum. Nat Phys. 2011;7:527–530.

[38] Gieseler J, Deutsch B, Quidant R, et al. Subkelvin parametric feedback cooling of a laser-trapped nanoparticle. Phys Rev Lett. 2012;109:103603.

[39] Kiesel N, Blaser F, Delić U, et al. Cavity cooling of an optically levitated submicron particle. Proc Natl Acad Sci USA. 2013;110:14180–14185.

[40] Windey D, Gonzalez-Ballestero C, Maurer P, et al. Cavity-based 3D cooling of a levitated nanoparticle via coherent scattering. Phys Rev Lett. 2019;122:123601.

[41] Delić U, Reisenbauer M, Grass D, et al. Cavity cooling of a levitated nanosphere by coherent scattering. Phys Rev Lett. 2019;122:123602.

[42] Conangla GP, Ricci F, Cuairan MT, et al. Optimal feedback cooling of a charged levitated nanoparticle with adaptive control. Phys Rev Lett. 2019;122:223602.

[43] Tebbenjohanns F, Frimmer M, Militaru A, et al. Cold damping of an optically levitated nanoparticle to microkelvin temperatures. Phys Rev Lett. 2019;122:223601.

[44] Delić U, Reisenbauer M, Dare K, et al. Cooling of a levitated nanoparticle to the motional quantum ground state. Science. 2020;367:892–895.

[45] Būtaitė UG, Gibson GM, Ho YLD, et al. Indirect optical trapping using light driven micro-rotors for reconfigurable hydrodynamic manipulation. Nat Commun. 2019;10:1215.

[46] Wu T, Nieminen TA, Mohanty S, et al. A photon-driven micromotor can direct nerve fibre growth. Nat Photonics. 2012;6:62–67.

[47] Ramaiya A, Roy B, Bugiel M, et al. Kinesin rotates unidirectionally and generates torque while walking on microtubules. Proc Natl Acad Sci USA. 2017;114:10894–10899.

[48] Padgett M, Bowman R. Tweezers with a twist. Nat Photonics. 2011;5:343–348.

[49] Ahn J, Xu Z, Bang J, et al. Ultrasensitive torque detection with an optically levitated nanorotor. Nat Nanotechnol. 2020;15:89–93.

[50] Skelton Spesyvtseva SE, Dholakia K. Trapping in a material world. ACS Photonics. 2016;3:719–736.

[51] Manjavacas A, García De Abajo FJ. Vacuum friction in rotating particles. Phys Rev Lett. 2010;105:113601.

[52] Manjavacas A, García De Abajo FJ. Thermal and vacuum friction acting on rotating particles. Phys Rev A. 2010;82:063827.

[53] Zhao R, Manjavacas A, García De Abajo FJ, et al. Rotational quantum friction. Phys Rev Lett. 2012;109:123604.

[54] Beresnev SA, Chernyak VG, Fomyagin GA. Motion of a spherical particle in a rarefied gas. Part 2. Drag and thermal polarization. J Fluid Mech. 1990;219:405–421.

[55] Kuhn S, Asenbaum P, Kosloff A, et al. Cavity-assisted manipulation of freely rotating silicon nanorods in high vacuum. Nano Lett. 2015;15:5604–5608.

[56] Wang K, Schonbrun E, Steinvurzel P, et al. Trapping and rotating nanoparticles using a plasmonic nano-tweezer with an integrated heat sink. Nat Commun. 2011;2:469.

[57] Biswas T, Kani A, Bhattacharya M. Rotating levitated nanoparticle sensors in a hollow-core photonic crystal fiber. J Opt Soc Am B. 2020;37:1598–1605.

[58] Tkachenko G, Toftul I, Esporlas C, et al. Light-induced rotation of dielectric micro-particles around an optical nanofiber. Optica. 2020;7:59–62.

[59] Arnold S, Keng D, Shopova SI, et al. Whispering gallery mode carousel – a photonic mechanism for enhanced nanoparticle detection in biosensing. Opt Express. 2009;17:6230–6238.

[60] Zou X, Zheng Q, Wu D, et al. Controllable cellular micromotors based on optical tweezers. Adv Funct Mater. 2020;30:2002081.

[61] Rodríguez-Sevilla P, Labrador-Páez L, Wawrzyńczyk D, et al., et al. Determining the 3D orientation of optically trapped upconverting nanorods by in situ single-particle polarized spectroscopy. Nanoscale. 2016;8:300–308.

[62] Lenton ICD, Armstrong DJ, Stilgoe AB, et al. Orientation of swimming cells with annular beam optical tweezers. Opt Commun. 2020;459:124864.

[63] Čižmár T, Brzobohatý O, Dholakia K, et al. The holographic optical micro-manipulation system based on counter-propagating beams. Laser Phys Lett. 2010;8:50–56.

[64] Paterson L, MacDonald MP, Arlt J, et al. Controlled rotation of optically trapped microscopic particles. Science. 2001;292:912–914.

[65] Zhang P, Hernandez D, Cannan D, et al. Trapping and rotating microparticles and bacteria with Moiré-based optical propelling beams. Biomed Opt Express. 2012;3:1891–1897.

[66] MacDonald MP, Paterson L, Volke-Sepulveda K, et al. Creation and manipulation of three-dimensional optically trapped structures. Science. 2002;296:1101–1103.

[67] Franke-Arnold S, Leach J, Padgett MJ, et al. Optical Ferris wheel for ultracold atoms. Opt Express. 2007;15:8619–8625.

[68] Bezryadina AS, Preece DC, Chen JC, et al. Optical disassembly of cellular clusters by tunable 'tug-of-war' tweezers. Light Sci Appl. 2016;5:e16158.

[69] Roichman Y, Sun B, Stolarski A, et al. Influence of nonconservative optical forces on the dynamics of optically trapped colloidal spheres: the fountain of probability. Phys Rev Lett. 2008;101:128301.

[70] Cheng Z, Chaikin PM, Mason TG. Light streak tracking of optically trapped thin microdisks. Phys Rev Lett. 2002;89:108303.

[71] Cheng Z, Mason TG, Chaikin PM. Periodic oscillation of a colloidal disk near a wall in an optical trap. Phys Rev E. 2003;68:051404.

[72] Mihiretie BM, Snabre P, Loudet JC, et al. Radiation pressure makes ellipsoidal particles tumble. EPL. 2012;100:48005.

[73] Leach J, Mushfique H, Keen S, et al. Comparison of Faxén's correction for a microsphere translating or rotating near a surface. Phys Rev E. 2009;79:026301.

[74] Stickler BA, Nimmrichter S, Martinetz L, et al. Rotranslational cavity cooling of dielectric rods and disks. Phys Rev A. 2016;94:033818.

[75] Hoang TM, Ma Y, Ahn J, et al. Torsional optomechanics of a levitated nonspherical nanoparticle. Phys Rev Lett. 2016;117:1223604.

[76] La Porta A, Wang MD. Optical torque wrench: angular trapping, rotation, and torque detection of quartz microparticles. Phys Rev Lett. 2004;92:190801.

[77] Friese M, Nieminen T, Heckenberg N, et al. Optical alignment and spinning of laser-trapped microscopic particles. Nature. 1998;394:348–350.

[78] Nieminen TA, Heckenberg NR, Rubinsztein-dunlop H. Optical measurement of microscopic torques. J Mod Opt. 2001;48:405–413.

[79] Simpson SH. Inhomogeneous and anisotropic particles in optical traps: physical behaviour and applications. J Quant Spectrosc Radiat Transf. 2014;146:81–99.

[80] Higurashi E, Sawada R, Ito T. Optically induced angular alignment of trapped birefringent micro-objects by linearly polarized light. Phys Rev E. 1999;59:3676–3681.

[81] Ahn J, Xu Z, Bang J, et al. Optically levitated nanodumbbell torsion balance and GHz nanomechanical rotor. Phys Rev Lett. 2018;121:33603.

[82] Kuhn S, Kosloff A, Stickler BA, et al. Full rotational control of levitated silicon nanorods. Optica. 2017;4:356.

[83] Rahman AA, Barker P. Laser refrigeration, alignment and rotation of levitated Yb^{3+}: YLF nanocrystals. Nat Photonics. 2017;11:634.

[84] Zhong C, Robicheaux F. Shot-noise-dominant regime for ellipsoidal nanoparticles in a linearly polarized beam. Phys Rev A. 2017;95:053421.

[85] Bonin KD, Kourmanov B, Walker TG. Light torque nanocontrol, nanomotors and nanorockers. Opt Express. 2002;10:984–989.

[86] Tong L, Miljković VD, Käll M. Alignment, rotation, and spinning of single plasmonic nanoparticles and nanowires using polarization dependent optical forces. Nano Lett. 2010;10:268–273.

[87] Wulff KD, Cole DG, Clark RL. Controlled rotation of birefringent particles in an optical trap. Appl Opt. 2008;47:6428–6433.

[88] Beth RA. Mechanical detection and measurement of the angular momentum of light. Phys Rev. 1936;50:115.

[89] Friese MEJ, Enger J, Rubinsztein-Dunlop H, et al. Optical angular-momentum transfer to trapped absorbing particles. Phys Rev A. 1996;54:1593–1596.

[90] Lehmuskero A, Ogier R, Gschneidtner T, et al. Ultrafast spinning of gold nanoparticles in water using circularly polarized light. Nano Lett. 2013;13:3129–3134.

[91] Marston PL, Crichton JH. Radiation torque on a sphere caused by a circularly-polarized electromagnetic wave. Phys Rev A. 1984;30:2508–2516.

[92] Shao L, Yang ZJ, Andrén D, et al. Gold nanorod rotary motors driven by resonant light scattering. ACS Nano. 2015;9:12542–12551.

[93] Runowski M, Woźny P, Lis S, et al. Optical vacuum sensor based on lanthanide upconversion—luminescence thermometry as a tool for ultralow pressure sensing. Adv Mater Technol. 2020;5:1901091.

[94] Courtial J, Padgett MJ. Limit to the orbital angular momentum per unit energy in a light beam that can be focussed onto a small particle. Opt Commun. 2000;173:269–274.

[95] Lehmuskero A, Li Y, Johansson P, et al. Plasmonic particles set into fast orbital motion by an optical vortex beam. Opt Express. 2014;22:4349–4356.

[96] Allen L, Beijersbergen MW, Spreeuw RJC, et al. Orbital angular momentum of light and the transformation of Laguerre-Gaussian laser modes. Phys Rev A. 1992;45:8185–8189.

[97] O'Neil AT, MacVicar I, Allen L, et al. Intrinsic and extrinsic nature of the orbital angular momentum of a light beam. Phys Rev Lett. 2002;88:053601.

[98] O'Neil AT, Padgett MJ. Three-dimensional optical confinement of micron-sized metal particles and the decoupling of the spin and orbital angular momentum within an optical spanner. Opt Commun. 2000;185:139–143.

[99] Zhao Y, Edgar JS, Jeffries GDM, et al. Spin-to-orbital angular momentum conversion in a strongly focused optical beam. Phys Rev Lett. 2007;99:073901.

[100] Volke-Sepulveda K, Garcés-Chávez V, Chávez-Cerda S, et al. Orbital angular momentum of a high-order Bessel light beam. J Opt B: Quant Semiclass. 2002;4:S82–S89.

[101] Garcés-Chávez V, McGloin D, Padgett M, et al. Observation of the transfer of the local angular momentum density of a multiringed light beam to an optically trapped particle. Phys Rev Lett. 2003;91:093602.

[102] He H, Friese ME, Heckenberg NR, et al. Direct observation of transfer of angular momentum to absorptive particles from a laser beam with a phase singularity. Phys Rev Lett. 1995;75:826–829.

[103] Simpson NB, Dholakia K, Allen L, et al. Mechanical equivalence of spin and orbital angular momentum of light: an optical spanner. Opt Lett. 1997;22:52–54.

[104] Dienerowitz M, Mazilu M, Reece PJ, et al. Optical vortex trap for resonant confinement of metal nanoparticles. Opt Express. 2008;16:4991–4999.

[105] Grier DG. A revolution in optical manipulation. Nature. 2003;424:810–816.

[106] Dholakia K, Čižmár T. Shaping the future of manipulation. Nat Photonics. 2011;5:335–342.

[107] Padgett MJ. Orbital angular momentum 25 years on. Opt Express. 2017;25: 11265–11274.

[108] Wang X, Nie Z, Liang Y, et al. Recent advances on optical vortex generation. Nanophotonics. 2018;7:1533–1556.

[109] Dickey FM. Laser beam shaping: theory and techniques. Boca Raton, FL: CRC press; 2018.

[110] Forbes A. Structured light from lasers. Laser Photonics Rev. 2019;13:1900140.

[111] Rubinsztein-Dunlop H, Forbes A, Berry MV, et al. Roadmap on structured light. J Opt. 2016;19:013001.

[112] Shen Y, Wang X, Xie Z, et al. Optical vortices 30 years on: OAM manipulation from topological charge to multiple singularities. Light Sci Appl. 2019;8:1–29.

[113] Donato MG, Brzobohatý O, Simpson SH, et al. Optical trapping, optical binding, and rotational dynamics of silicon nanowires in counter-propagating beams. Nano Lett. 2019;19:342–352.

[114] Marrucci L, Manzo C, Paparo D. Optical spin-to-orbital angular momentum conversion in inhomogeneous anisotropic media. Phys Rev Lett. 2006;96:163905.

[115] Nieminen TA, Stilgoe AB, Heckenberg NR, et al. Angular momentum of a strongly focused Gaussian beam. J Opt A: Pure Appl Opt. 2008;10:115005.

[116] Li M, Cai Y, Yan S, et al. Orbit-induced localized spin angular momentum in strong focusing of optical vectorial vortex beams. Phys Rev A. 2018;97:053842.

[117] Zhao Y, Shapiro D, McGloin D, et al. Direct observation of the transfer of orbital angular momentum to metal particles from a focused circularly polarized Gaussian beam. Opt Express. 2009;17:23316–23322.

[118] Ranjit G, Montoya C, Geraci AA. Cold atoms as a coolant for levitated optomechanical systems. Phys Rev A. 2015;91:013416.

[119] Koya AN, Cunha J, Guo TL, et al. Novel plasmonic nanocavities for optical trapping-assisted biosensing applications. Adv Opt Mater. 2020;8:1901481.

[120] Lei H, Zhang Y, Li X, et al. Photophoretic assembly and migration of dielectric particles and escherichia coli in liquids using a subwavelength diameter optical fiber. Lab Chip. 2011;11:2241–2246.

[121] Frawley MC, Gusachenko I, Truong VG, et al. Selective particle trapping and optical binding in the evanescent field of an optical nanofiber. Opt Express. 2014;22: 16322–16334.

[122] Constable A, Kim J, Mervis J, et al. Demonstration of a fiber-optical light-force trap. Opt Lett. 1993;18:1867–1869.

[123] Xiao G, Yang K, Luo H, et al. Orbital rotation of trapped particle in a transversely misaligned dual-fiber optical trap. IEEE Photon J. 2016;8:6100108.

[124] Blakely JT, Gordon R, Sinton D. Flow-dependent optofluidic particle trapping and circulation. Lab Chip. 2008;8:1350–1356.

[125] Kreysing MK, Kießling T, Fritsch A, et al. The optical cell rotator. Opt Express. 2008;16:16984–16992.

[126] Brzobohatý O, Arzola AV, Šiler M, et al. Complex rotational dynamics of multiple spheroidal particles in a circularly polarized, dual beam trap. Opt Express. 2015;23:7273–7287.

[127] Wilson BK, Mentele T, Bachar S, et al. Nanostructure-enhanced laser tweezers for efficient trapping and alignment of particles. Opt Express. 2010;18:16005–16013.

[128] Liu M, Zentgraf T, Liu Y, et al. Light-driven nanoscale plasmonic motors. Nat Nanotechnol. 2010;5:570–573.

[129] Tsai WY, Huang JS, Huang CB. Selective trapping or rotation of isotropic dielectric microparticles by optical near field in a plasmonic Archimedes spiral. Nano Lett. 2014;14:547–552.

[130] Rodrigo JA, Alieva T. Freestyle 3D laser traps: tools for studying light-driven particle dynamics and beyond. Optica. 2015;2:812–815.

[131] Ladavac K, Grier DG. Colloidal hydrodynamic coupling in concentric optical vortices. EPL. 2005;70:548–554.

[132] Shen Z, Su L, Yuan XC, et al. Trapping and rotating of a metallic particle trimer with optical vortex. Appl Phys Lett. 2016;109:241901.

[133] Tao SH, Yuan XC, Lin J, et al. Influence of geometric shape of optically trapped particles on the optical rotation induced by vortex beams. J Appl Phys. 2006;100:043105.

[134] Burns MM, Fournier JM, Golovchenko JA. Optical binding. Phys Rev Lett. 1989;63:1233–1236.

[135] Haefner D, Sukhov S, Dogariu A. Conservative and nonconservative torques in optical binding. Phys Rev Lett. 2009;103:173602.

[136] Liaw JW, Huang MC, Chao HY, et al. Spin and orbital rotation of plasmonic dimer driven by circularly polarized light. Nanoscale Res Lett. 2018;13:322.

[137] Sule N, Yifat Y, Gray SK, et al. Rotation and negative torque in electrodynamically bound nanoparticle dimers. Nano Lett. 2017;17:6548–6556.

[138] Han F, Parker JA, Yifat Y, et al. Crossover from positive to negative optical torque in mesoscale optical matter. Nat Commun. 2018;9:4897.

[139] Tamura M, Omatsu T, Tokonami S, et al. Interparticle-interaction-mediated anomalous acceleration of nanoparticles under light-field with coupled orbital and spin angular momentum. Nano Lett. 2019;19:4873–4878.

[140] Deufel C, Forth S, Simmons CR, et al. Nanofabricated quartz cylinders for angular trapping: DNA supercoiling torque detection. Nat Methods. 2007;4:223–225.

[141] Bishop AI, Nieminen TA, Heckenberg NR, et al. Optical microrheology using rotating laser-trapped particles. Phys Rev Lett. 2004;92:198104.

[142] Knöner G, Parkin S, Heckenberg NR, et al. Characterization of optically driven fluid stress fields with optical tweezers. Phys Rev E. 2005;72:031507.

[143] Leach J, Mushfique H, Di Leonardo R, et al. An optically driven pump for microfluidics. Lab Chip. 2006;6:735–739.

[144] Arita Y, McKinley AW, Mazilu M, et al. Picoliter rheology of gaseous media using a rotating optically trapped birefringent microparticle. Anal Chem. 2011;83:8855–8858.

[145] Arita Y, Mazilu M, Dholakia K. Laser-induced rotation and cooling of a trapped microgyroscope in vacuum. Nat Commun. 2013;4:2374.

[146] Monteiro F, Ghosh S, Van Assendelft EC, et al. Optical rotation of levitated spheres in high vacuum. Phys Rev A. 2018;97:51802.

[147] Arita Y, Richards JM, Mazilu M, et al. Rotational dynamics and heating of trapped nanovaterite particles. ACS Nano. 2016;10:11505–11510.

[148] Fernández-Nieves A, Cristobal G, Garcés-Chávez V, et al. Optically anisotropic colloids of controllable shape. Adv Mater. 2005;17:680–684.

[149] Wood TA, Gleeson HF, Dickinson MR, et al. Mechanisms of optical angular momentum transfer to nematic liquid crystalline droplets. Appl Phys Lett. 2004;84:4292–4294.

[150] Roder PB, Smith BE, Zhou X, et al. Laser refrigeration of hydrothermal nanocrystals in physiological media. Proc Natl Acad Sci USA. 2015;112:15024–15029.

[151] Rodríguez-Sevilla P, Lee T, Liang L, et al. Light-activated upconverting spinners. Adv Opt Mater. 2018;6:1800161.

[152] Rodríguez-Sevilla P, Arita Y, Liu X, et al. The temperature of an optically trapped, rotating microparticle. ACS Photonics. 2018;5:3772–3778.

[153] Ha S, Tang Y, van Oene MM, et al. Single-crystal rutile TiO2 nanocylinders are highly effective transducers of optical force and torque. ACS Photonics. 2019;6:1255–1265.

[154] Jaque D, Martínez Maestro L, Del Rosal B, et al. Nanoparticles for photothermal therapies. Nanoscale. 2014;6:9494–9530.

[155] Abbas MM, Craven PD, Spann JF, et al. Laboratory experiments on rotation and alignment of the analogs of interstellar dust grains by radiation. Astrophys J. 2004;614:781–795.

[156] Galajda P, Ormos P. Orientation of flat particles in optical tweezers by linearly polarized light. Opt Express. 2003;11:446–451.

[157] Singer W, Nieminen TA, Gibson UJ, et al. Orientation of optically trapped nonspherical birefringent particles. Phys Rev E. 2006;73:021911.

[158] Neale SL, MacDonald MP, Dholakia K, et al. All-optical control of microfluidic components using form birefringence. Nat Mater. 2005;4:530–533.

[159] Galajda P, Ormos P. Complex micromachines produced and driven by light. Appl Phys Lett. 2001;78:249–251.

[160] Higurashi E, Ukita H, Tanaka H, et al. Optically induced rotation of anisotropic micro-objects fabricated by surface micromachining. Appl Phys Lett. 1994;64:2209–2210.

[161] Galajda P, Ormos P. Rotors produced and driven in laser tweezers with reversed direction of rotation. Appl Phys Lett. 2002;80:4653–4655.

[162] Swartzlander Jr GA, Peterson TJ, Artusio-Glimpse AB, et al. Stable optical lift. Nat Photonics. 2011;5:48.

[163] Asavei T, Loke VLY, Barbieri M, et al. Optical angular momentum transfer to microrotors fabricated by two-photon photopolymerization. New J Phys. 2009;11:093021.

[164] Svenskaya YI, Fattah H, Inozemtseva OA, et al. Key parameters for size- and shape-controlled synthesis of vaterite particles. Cryst Growth Des. 2018;18:331–337.

[165] Liu D, Xu X, Du Y, et al. Three-dimensional controlled growth of monodisperse sub-50 nm heterogeneous nanocrystals. Nat Commun. 2016;7:10254.

[166] Lee YJ, Schade NB, Sun L, et al. Ultrasmooth, highly spherical monocrystalline gold particles for precision plasmonics. ACS Nano. 2013;7:11064–11070.

[167] Rashid M, Toroš M, Setter A, et al. Precession motion in levitated optomechanics. Phys Rev Lett. 2018;121:253601.

[168] Ilic O, Kaminer I, Zhen B, et al. Topologically enabled optical nanomotors. Sci Adv. 2017;3:e1602738.

[169] Zong Y, Liu J, Liu R, et al. An optically driven bistable Janus rotor with patterned metal coatings. ACS Nano. 2015;9:10844–10851.

[170] Hernández RJ, Mazzulla A, Provenzano C, et al. Chiral resolution of spin angular momentum in linearly polarized and unpolarized light. Sci Rep. 2015;5:16926.

[171] Martinetz L, Hornberger K, Stickler BA. Gas-induced friction and diffusion of rigid rotors. Phys Rev E. 2018;97:052112.

[172] Reimann R, Doderer M, Hebestreit E, et al. GHz rotation of an optically trapped nanoparticle in vacuum. Phys Rev Lett. 2018;121:33602.

[173] Nagornykh P, Coppock JE, Murphy JPJ, et al. Optical and magnetic measurements of gyroscopically stabilized graphene nanoplatelets levitated in an ion trap. Phys Rev B. 2017;96:035402.

[174] Schuck M, Steinert D, Nussbaumer T, et al. Ultrafast rotation of magnetically levitated macroscopic steel spheres. Sci Adv. 2018;4:e1701519.

[175] Hümmer D, Lampert R, Kustura K, et al. Acoustic and optical properties of a fast-spinning dielectric nanoparticle. Phys Rev B. 2020;101:205416.

[176] Mazilu M, Arita Y, Vettenburg T, et al. Orbital-angular-momentum transfer to optically levitated microparticles in vacuum. Phys Rev A. 2016;94:053821.

[177] Svak V, Brzobohatý O, Šiler M, et al. Transverse spin forces and non-equilibrium particle dynamics in a circularly polarized vacuum optical trap. Nat Commun. 2018;9:5453.

[178] Arita Y, Chen M, Wright EM, et al. Dynamics of a levitated microparticle in vacuum trapped by a perfect vortex beam: three-dimensional motion around a complex optical potential. J Opt Soc Am B. 2017;34:C14–C19.

[179] Chen X, Xiao G, Xiong W, et al. Rotation of an optically trapped vaterite microsphere measured using rotational Doppler effect. Opt Eng. 2018;57:036103.

[180] Bishop AI, Nieminen TA, Heckenberg NR, et al. Optical application and measurement of torque on microparticles of isotropic nonabsorbing material. Phys Rev A. 2003;68:033802.

[181] Volpe G, Petrov D. Torque detection using Brownian fluctuations. Phys Rev Lett. 2006;97:210603.

[182] Bliokh KY, Bekshaev AY, Nori F. Extraordinary momentum and spin in evanescent waves. Nat Commun. 2014;5:3300.

[183] Angelsky OV, Bekshaev AY, Maksimyak PP, et al. Orbital rotation without orbital angular momentum: mechanical action of the spin part of the internal energy flow in light beams. Opt Express. 2012;20:3563–3571.

[184] Roy B, Ghosh N, Banerjee A, et al. Manifestations of geometric phase and enhanced spin Hall shifts in an optical trap. New J Phys. 2014;16:083037.

[185] Arzola AV, Chvátal L, Jákl P, et al. Spin to orbital light momentum conversion visualized by particle trajectory. Sci Rep. 2019;9:4127.

[186] Gooding C, Weinfurtner S, Unruh WG. Reinventing the Zel'Dovich wheel. Phys Rev A. 2020;101:063819.

[187] Braidotti MC, Vinante A, Gasbarri G, et al. Zel'Dovich amplification in a superconducting circuit. arXiv. 2020;2005:03705.

[188] Mushfique H, Leach J, Di Leonardo R, et al. Optically driven pumps and flow sensors for microfluidic systems. Proc Inst Mech Eng Part C. 2008;222:829–837.

[189] Špová-Jungová H, Andrén D, Jones S, et al. Nanoscale inorganic motors driven by light: principles, realizations, and opportunities. Chem Rev. 2020;120:269–287.

[190] Li Y, Liu X, Xu X, et al. Red-blood-cell waveguide as a living biosensor and micromotor. Adv Funct Mater. 2019;29:1905568.

[191] Zheng J, Xing X, Yang J, et al. Hybrid optofluidics and three-dimensional manipulation based on hybrid photothermal waveguides. NPG Asia Mater. 2018;10:340–351.

[192] Ronzani A, Karimi B, Senior J, et al. Tunable photonic heat transport in a quantum heat valve. Nat Phys. 2018;14:991–995.
[193] Klatzow J, Becker JN, Ledingham PM, et al. Experimental demonstration of quantum effects in the operation of microscopic heat engines. Phys Rev Lett. 2019;122:110601.
[194] Maslennikov G, Ding S, Hablützel R, et al. Quantum absorption refrigerator with trapped ions. Nat Commun. 2019;10:202.
[195] Mitchison MT. Quantum thermal absorption machines: refrigerators, engines and clocks. Contemp Phys. 2019;60:164–187.
[196] Gieseler J, Millen J. Levitated nanoparticles for microscopic thermodynamics - a review. Entropy. 2018;20:326.
[197] Roulet A, Nimmrichter S, Arrazola JM, et al. Autonomous rotor heat engine. Phys Rev E. 2017;95:062131.
[198] Arita Y, Simpson SH, Zemánek P, et al. Coherent oscillations of a levitated birefringent microsphere in vacuum driven by nonconservative rotation-translation coupling. Sci Adv. 2020;6:eaaz9858.
[199] Irrera A, Magazzú A, Artoni P, et al. Photonic torque microscopy of the non-conservative force field for optically trapped silicon nanowires. Nano Lett. 2016;16:4181–4188.
[200] Liu Z, Leong J, Nimmrichter S, et al. Quantum gears from planar rotors. Phys Rev E. 2019;99:042202.
[201] Arita Y, Mazilu M, Vettenburg T, et al. Rotation of two trapped microparticles in vacuum: observation of optically mediated parametric resonances. Opt Lett. 2015;40:4751.
[202] Arita Y, Wright EM, Dholakia K. Optical binding of two cooled micro-gyroscopes levitated in vacuum. Optica. 2018;5:910.
[203] Kalwarczyk T, Ziębacz N, Bielejewska A, et al. Comparative analysis of viscosity of complex liquids and cytoplasm of mammalian cells at the nanoscale. Nano Lett. 2011;11:2157–2163.
[204] Wirtz D. Particle-tracking microrheology of living cells: principles and applications. Annu Rev Biophys. 2009;38:301–326.
[205] Robertson-Anderson RM. Optical tweezers microrheology: from the basics to advanced techniques and applications. ACS Macro Lett. 2018;7:968–975.
[206] Vaippully R, Ramanujan V, Bajpai S, et al. Measurement of viscoelastic properties of the cellular cytoplasm using optically trapped Brownian probes. J Phys: Condens Matter. 2020;32:235101.
[207] Blehm BH, Devine A, Staunton JR, et al. In vivo tissue has non-linear rheological behavior distinct from 3D biomimetic hydrogels, as determined by amotiv microscopy. Biomaterials. 2016;83:66–78.
[208] Arzola AV, Jákl P, Chvátal L, et al. Rotation, oscillation and hydrodynamic synchronization of optically trapped oblate spheroidal microparticles. Opt Express. 2014;22:16207–16221.
[209] Kraft DJ, Wittkowski R, Ten Hagen B, et al. Brownian motion and the hydrodynamic friction tensor for colloidal particles of complex shape. Phys Rev E. 2013;88:050301.
[210] Kern M, Jeske J, Lau DWM, et al. Optical cryocooling of diamond. Phys Rev B. 2017;95:235306.
[211] Blakemore CP, Martin D, Fieguth A, et al. Absolute pressure and gas species identification with an optically levitated rotor. J Vac Sci Technol B. 2020;38:024201.
[212] Maxwell JC. On the viscosity or internal friction of air and other gases. Philos Trans Royal Soc (London). 1866;156:249–268.

[213] Kuhn S, Stickler BA, Kosloff A, et al. Optically driven ultra-stable nanomechanical rotor. Nat Commun. 2017;8:1670.

[214] Rider AD, Blakemore CP, Kawasaki A, et al. Electrically driven, optically levitated microscopic rotors. Phys Rev A. 2019;99:041802.

[215] Moore RW, Lee LA, Findlay EA, et al. Measurement of vacuum pressure with a magneto-optical trap: a pressure-rise method. Rev Sci Instrum. 2015;86:093108.

[216] Eckel S, Barker DS, Fedchak JA, et al. Challenges to miniaturizing cold atom technology for deployable vacuum metrology. Metrologia. 2018;55:S182.

[217] Rings D, Selmke M, Cichos F, et al. Theory of hot Brownian motion. Soft Matter. 2011;7:3441–3452.

[218] Rings D, Chakraborty D, Kroy K. Rotational hot Brownian motion. New J Phys. 2012;14:053012.

[219] Srivastava M, Chakraborty D. The effective temperature for the thermal fluctuations in hot Brownian motion. J Chem Phys. 2018;148:204902.

[220] Hajizadeh F, Shao L, Andrén D, et al. Brownian fluctuations of an optically rotated nanorod. Optica. 2017;4:746–751.

[221] Millen J, Deesuwan T, Barker P, et al. Nanoscale temperature measurements using non-equilibrium Brownian dynamics of a levitated nanosphere. Nat Nanotechnol. 2014;9:425.

[222] Hebestreit E, Reimann R, Frimmer M, et al. Measuring the internal temperature of a levitated nanoparticle in high vacuum. Phys Rev A. 2018;97:043803.

[223] Seletskiy DV, Melgaard SD, Bigotta S, et al. Laser cooling of solids to cryogenic temperatures. Nat Photonics. 2010;4:161–164.

[224] Melgaard SD, Albrecht AR, Hehlen MP, et al. Solid-state optical refrigeration to sub-100 Kelvin regime. Sci Rep. 2016;6:20380.

[225] van der Laan F, Reimann R, Militaru A, et al. Optically levitated rotor at its thermal limit of frequency stability. Phys Rev A. 2020;102:013505.

[226] Seberson T, Robicheaux F. Stability and dynamics of optically levitated dielectric disks in a gaussian standing wave beyond the harmonic approximation. Phys Rev Res. 2020;2:033437.

[227] Shi H, Bhattacharya M. Optomechanics based on angular momentum exchange between light and matter. J Phys B: At Mol Opt Phys. 2016;49:153001.

[228] Liu S, Li T, Yin Z. Coupling librational and translational motion of a levitated nanoparticle in an optical cavity. J Opt Soc Am B. 2017;34:C8–C13.

[229] Ralph JF, Jacobs K, Coleman J. Coupling rotational and translational motion via a continuous measurement in an optomechanical sphere. Phys Rev A. 2016;94:032108.

[230] Seberson T, Robicheaux F. Parametric feedback cooling of rigid body nanodumbbells in levitated optomechanics. Phys Rev A. 2019;99:013821.

[231] Xu Z, Li T. Detecting Casimir torque with an optically levitated nanorod. Phys Rev A. 2017;96:33843.

[232] Arvanitaki A, Geraci AA. Detecting high-frequency gravitational waves with optically levitated sensors. Phys Rev Lett. 2013;110:071105.

[233] Bang J, Seberson T, Ju P, et al. 5D cooling and nonlinear dynamics of an optically levitated nanodumbbell. arXiv. 2020;2004:02384.

[234] Pan D, Xu H, de Abajo F. Rotational Doppler cooling and heating. arXiv. 2019;1908:07973.

[235] Seberson T, Ahn J, Bang J, et al. Optical levitation of a YIG nanoparticle and simulation of sympathetic cooling via coupling to a cold atomic gas. arXiv. 2019;1910:05371.

[236] Hopper A, Barker P. A hybrid quantum system formed by trapping atoms in the near-field of a levitated nanosphere. arXiv. 2020;2005:11662.

[237] Scala M, Kim MS, Morley GW, et al. Matter-wave interferometry of a levitated thermal nano-oscillator induced and probed by a spin. Phys Rev Lett. 2013;111: 180403.

[238] Delord T, Nicolas L, Chassagneux Y, et al. Strong coupling between a single nitrogen-vacancy spin and the rotational mode of diamonds levitating in an ion trap. Phys Rev A. 2017;96:063810.

[239] Ma Y, Hoang TM, Gong M, et al. Proposal for quantum many-body simulation and torsional matter-wave interferometry with a levitated nanodiamond. Phys Rev A. 2017;96:023827.

[240] Ge L, Zhao N. Torsional cooling of a nanodiamond via the interaction with the electron spin of the embedded nitrogen-vacancy center. Phys Rev A. 2018;98:043415.

[241] Delord T, Huillery P, Nicolas L, et al. Spin-cooling of the motion of a trapped diamond. Nature. 2020;580:56–59.

[242] Metcalf HJ. van der Straten P. Laser cooling and trapping of atoms. J Opt Soc Am B. 2003;20:887–908.

[243] Eschner J, Morigi G, Schmidt-Kaler F, et al. Laser cooling of trapped ions. J Opt Soc Am B. 2003;20:1003–1015.

[244] Leibfried D, Blatt R, Monroe C, et al. Quantum dynamics of single trapped ions. Rev Mod Phys. 2003;75:281–324.

[245] Huillery P, Delord T, Nicolas L, et al. Spin mechanics with levitating ferromagnetic particles. Phys Rev B. 2020;101:134415.

[246] Bryant Z, Stone MD, Gore J, et al. Structural transitions and elasticity from torque measurements on DNA. Nature. 2003;424:338–341.

[247] de Coulomb CA. Premier mémoire sur l'électricité et le magnétisme. Histoire de l'Académie Royale des Sciences. 1785;569–577.

[248] Cavendish H. Experiments to determine the density of the earth. Philos Trans Royal Soc (London). 1798;88:469–526.

[249] Lebedew P. Untersuchungen über die druckkräfte des lichtes. Ann Phys. 1901;311:433–458.

[250] Oroszi L, Galajda P, Kirei H, et al. Direct measurement of torque in an optical trap and its application to double-strand DNA. Phys Rev Lett. 2006;97:058301.

[251] Sheinin MY, Wang MD. Twist–stretch coupling and phase transition during DNA supercoiling. Phys Chem Chem Phys. 2009;11:4800–4803.

[252] Ma J, Bai L, Wang MD. Transcription under torsion. Science. 2013;340:1580.

[253] Moser J, Güttinger J, Eichler A, et al. Ultrasensitive force detection with a nanotube mechanical resonator. Nat Nanotechnol. 2013;8:493–496.

[254] Gieseler J, Novotny L, Quidant R. Thermal nonlinearities in a nanomechanical oscillator. Nat Phys. 2013;9:806–810.

[255] Hempston D, Vovrosh J, Toroš M, et al. Force sensing with an optically levitated charged nanoparticle. Appl Phys Lett. 2017;111:133111.

[256] Moore DC, Rider AD, Gratta G. Search for millicharged particles using optically levitated microspheres. Phys Rev Lett. 2014;113:251801.

[257] Rider AD, Moore DC, Blakemore CP, et al. Search for screened interactions associated with dark energy below the 100 μm length scale. Phys Rev Lett. 2016;117: 101101.

[258] Kim P, Hauer B, Doolin C, et al. Approaching the standard quantum limit of mechanical torque sensing. Nat Commun. 2016;7:13165.

[259] Losby JE, Sauer VT, Freeman MR. Recent advances in mechanical torque studies of small-scale magnetism. J Phys D: Appl Phys. 2018;51:483001.

[260] Chan H, Aksyuk V, Kleiman R, et al. Quantum mechanical actuation of microelectromechanical systems by the Casimir force. Science. 2001;291:1941–1944.

[261] Schäfer J, Rudolph H, Hornberger K, et al. Cooling nanorotors by elliptic coherent scattering. arXiv. 2020;2006:04090.

[262] Casimir HB. On the attraction between two perfectly conducting plates. Front Phys. 1948;100:61–63.

[263] Philbin TG, Leonhardt U. No quantum friction between uniformly moving plates. New J Phys. 2009;11:033035.

[264] Pendry JB. Quantum friction–fact or fiction? New J Phys. 2010;12:033028.

[265] Kardar M, Golestanian R. The "friction" of vacuum, and other fluctuation-induced forces. Rev Mod Phys. 1999;71:1233–1245.

[266] Pendry JB. Shearing the vacuum - quantum friction. J Phys: Condens Matter. 1997;9:10301–10320.

[267] Diehl R, Hebestreit E, Reimann R, et al. Optical levitation and feedback cooling of a nanoparticle at subwavelength distances from a membrane. Phys Rev A. 2018;98: 013851.

[268] Manjavacas A, Rodríguez-Fortuño FJ, García de Abajo FJ, et al. Lateral Casimir force on a rotating particle near a planar surface. Phys Rev Lett. 2017;118:133605.

[269] Jiang QD, Wilczek F. Axial Casimir force. Phys Rev B. 2019;99:165402.

[270] Ameri V, Eghbali-Arani M. Rotational synchronization of two noncontact nanoparticles. J Opt Soc Am B. 2017;34:2514–2518.

[271] Sanders S, Kort-Kamp WJ, Dalvit DA, et al. Nanoscale transfer of angular momentum mediated by the Casimir torque. Commun Phys. 2019;2:71.

[272] Nimmrichter S, Hornberger K. Macroscopicity of mechanical quantum superposition states. Phys Rev Lett. 2013;110:160403.

[273] Arndt M, Hornberger K. Testing the limits of quantum mechanical superpositions. Nat Phys. 2014;10:271–277.

[274] Schrinski B, Nimmrichter S, Stickler BA, et al. Macroscopicity of quantum mechanical superposition tests via hypothesis falsification. Phys Rev A. 2019; 100:032111.

[275] Kovachy T, Asenbaum P, Overstreet C, et al. Quantum superposition at the half-metre scale. Nature. 2015;528:530–533.

[276] Islam R, Ma R, Preiss PM, et al. Measuring entanglement entropy in a quantum many-body system. Nature. 2015;528:77–83.

[277] Fein YY, Geyer P, Zwick P, et al. Quantum superposition of molecules beyond 25 kDa. Nat Phys. 2019;15:1242–1245.

[278] Shayeghi A, Rieser P, Richter G, et al. Matter-wave interference of a native polypeptide. Nat Commun. 2020;11:1447.

[279] Ockeloen-Korppi C, Damskägg E, Pirkkalainen JM, et al. Stabilized entanglement of massive mechanical oscillators. Nature. 2018;556:478–482.

[280] Riedinger R, Wallucks A, Marinković I, et al. Remote quantum entanglement between two micromechanical oscillators. Nature. 2018;556:473–477.

[281] Libbrecht KG, Black ED. Toward quantum-limited position measurements using optically levitated microspheres. Phys Lett A. 2004;321:99–102.

[282] Degen CL, Reinhard F, Cappellaro P. Quantum sensing. Rev Mod Phys. 2017;89:035002.

[283] Acín A, Bloch I, Buhrman H, et al. The quantum technologies roadmap: a European community view. New J Phys. 2018;20:080201.

[284] O'Connell AD, Hofheinz M, Ansmann M, et al. Quantum ground state and single-phonon control of a mechanical resonator. Nature. 2010;464:697–703.

[285] Chan J, Alegre TM, Safavi-Naeini AH, et al. Laser cooling of a nanomechanical oscillator into its quantum ground state. Nature. 2011;478:89–92.

[286] Aspelmeyer M, Kippenberg TJ, Marquardt F. Cavity optomechanics. Rev Mod Phys. 2014;86:1391–1452.

[287] Millen J, Gieseler J. Single particle thermodynamics with levitated nanoparticles. In: Binder F, Correa LA, Gogolin C, et al., editors. Thermodynamics in the Quantum Regime. Vol. 195. Cham: Springer International Publishing; 2018. p. 853–885.

[288] Hebestreit E, Frimmer M, Reimann R, et al. Sensing static forces with free-falling nanoparticles. Phys Rev Lett. 2018;121:063602.

[289] Zhong C, Robicheaux F. Decoherence of rotational degrees of freedom. Phys Rev A. 2016;94:052109.

[290] Ni KK, Ospelkaus S, De Miranda M, et al. A high phase-space-density gas of polar molecules. Science. 2008;322:231–235.

[291] Shi H, Bhattacharya M. Coupling a small torsional oscillator to large optical angular momentum. J Mod Opt. 2013;60:382–386.

[292] Stickler BA, Papendell B, Kuhn S, et al. Probing macroscopic quantum superpositions with nanorotors. New J Phys. 2018;20:122001.

[293] Papendell B, Stickler BA, Hornberger K. Quantum angular momentum diffusion of rigid bodies. New J Phys. 2017;19:122001.

[294] Stickler BA, Schrinski B, Hornberger K. Rotational friction and diffusion of quantum rotors. Phys Rev Lett. 2018;121:40401.

[295] Robinett RW. Quantum wave packet revivals. Phys Rep. 2004;392:1–119.

[296] Carlesso M, Paternostro M, Ulbricht H, et al. When Cavendish meets Feynman: A quantum torsion balance for testing the quantumness of gravity. arXiv. 2017;1710:08695.

[297] Schrinski B, Stickler BA, Hornberger K. Collapse-induced orientational localization of rigid rotors. J Opt Soc Am B. 2017;34:C1.

[298] Collett B, Pearle P. Wavefunction collapse and random walk. Found Phys. 2003;33:1495–1541.

[299] Bera S, Motwani B, Singh TP, et al. A proposal for the experimental detection of CSL induced random walk. Sci Rep. 2015;5:7664.

[300] Carlesso M, Paternostro M, Ulbricht H, et al. Non-interferometric test of the continuous spontaneous localization model based on rotational optomechanics. New J Phys. 2018;20:083022.

[301] Stickler BA, Papendell B, Hornberger K. Spatio-orientational decoherence of nanoparticles. Phys Rev A. 2016;94:033828.

[302] Carlesso M, Naeij HR, Bassi A. A general approach toward rotational decoherence. arXiv. 2019;1912:08159.

[303] Pedernales JS, Cosco F, Plenio MB. Decoherence-free rotational degrees of freedom for quantum applications. Phys Rev Lett. 2020;125:090501.

[304] Kiałka F, Stickler BA, Hornberger K. Orbital angular momentum interference of trapped matter waves. Phys Rev Res. 2020;2:022030.

[305] Pritchard JD, Dinkelaker AN, Arnold AS, et al. Demonstration of an inductively coupled ring trap for cold atoms. New J Phys. 2012;14:103047.

[306] Helm JL, Rooney SJ, Weiss C, et al. Splitting bright matter-wave solitons on narrow potential barriers: quantum to classical transition and applications to interferometry. Phys Rev A. 2014;89:033610.

[307] Bowman D, Ireland P, Bruce GD, et al. Multi-wavelength holography with a single spatial light modulator for ultracold atom experiments. Opt Express. 2015;23: 8365–8372.

[308] Shore BW, Dömötör P, Sadurn E, et al. Scattering of a particle with internal structure from a single slit. New J Phys. 2015;17:013046.

[309] Xiao KW, Zhao N, Yin Z. Bistability and squeezing of the librational mode of an optically trapped nanoparticle. Phys Rev A. 2017;96:013837.

[310] Wood AA, Hollenberg LC, Scholten RE, et al. Observation of a quantum phase from classical rotation of a single spin. Phys Rev Lett. 2020;124:020401.

[311] Yin Z, Zhao N, Li T. Hybrid opto-mechanical systems with nitrogen-vacancy centers. Sci China: Phys Mech Astronomy. 2015;58:1–12.

[312] Pettit RM, Ge W, Kumar P, et al. An optical tweezer phonon laser. Nat Photonics. 2019;13:402–405.

[313] Cheng W, Tian T, Wang Z. Quantum beats and metrology in a rapidly rotating nitrogen-vacancy center. Eur Phys J D. 2019;73:171.

[314] Gennerich A. Optical tweezers. New York, NY: Springer; 2017.

[315] Kane BE. Levitated spinning graphene flakes in an electric quadrupole ion trap. Phys Rev B. 2010;82:115441.

[316] Meng L, Cai F, Li F, et al. Acoustic tweezers. J Phys D: Appl Phys. 2019;52:273001.

[317] Barnett SM, Allen L, Cameron RP, et al. On the natures of the spin and orbital parts of optical angular momentum. J Opt. 2016;18:064004.

[318] Beijersbergen M, Coerwinkel R, Kristensen M, et al. Helical-wavefront laser beams produced with a spiral phaseplate. Opt Commun. 1994;112:321–327.

[319] Curtis JE, Koss BA, Grier DG. Dynamic holographic optical tweezers. Opt Commun. 2002;207:169–175.

[320] Chen M, Mazilu M, Arita Y, et al. Dynamics of microparticles trapped in a perfect vortex beam. Opt Lett. 2013;38:4919–4922.

[321] Tkachenko G, Chen M, Dholakia K, et al. Is it possible to create a perfect fractional vortex beam? Optica. 2017;4:330–333.

[322] Roichman Y, Grier DG. Projecting extended optical traps with shape-phase holography. Opt Lett. 2006;31:1675–1677.

[323] Roichman Y, Sun B, Roichman Y, et al. Optical forces arising from phase gradients. Phys Rev Lett. 2008;100:013602.

[324] Lee SH, Roichman Y, Grier DG. Optical solenoid beams. Opt Express. 2010;18:6988–6993.

[325] Bowman D, Harte TL, Chardonnet V, et al. High-fidelity phase and amplitude control of phase-only computer generated holograms using conjugate gradient minimisation. Opt Express. 2017;25:11692–11700.

[326] Garcés-Chávez V, Quidant R, Reece PJ, et al. Extended organization of colloidal microparticles by surface plasmon polariton excitation. Phys Rev B. 2006;73:085417.

[327] Ploschner M, Mazilu M, Krauss TF, et al. Optical forces near a nanoantenna. J Nanophotonics. 2010;4:041570.

[328] Ortiz-Rivero E, Prorok K, Skowickł M, et al. Single-cell biodetection by upconverting microspinners. Small. 2019;15:1904154.

[329] Xie S, Pennetta R, Wang Z, et al. Sustained self-starting orbital motion of a glass-fiber "nanoengine" driven by photophoretic forces. ACS Photonics. 2019;6:3315–3320.

[330] Childress L, Schmidt MP, Kashkanova AD, et al. Cavity optomechanics in a levitated helium drop. Phys Rev A. 2017;96:063842.